

Structure and Vibrational Spectrum of Formate and Acetate Adsorbed from Aqueous Solution onto the TiO₂ Rutile (110) Surface

François P. Rotzinger,^{*,†} Janet M. Kesselman-Truttmann,[‡] Stephan J. Hug,^{*,‡} Valery Shklover,[§] and Michael Grätzel[†]

Institut de chimie moléculaire et biologique, Ecole Polytechnique Fédérale, CH-1015 Lausanne, Switzerland, Swiss Federal Institute for Environmental Science and Technology, CH-8600 Dübendorf, Switzerland, and Laboratory of Crystallography, Swiss Federal Institute of Technology, CH-8092 Zürich, Switzerland

Received: July 18, 2003; In Final Form: November 5, 2003

The adsorption of formate and acetate from aqueous solutions at pH 3–9 onto the TiO₂ rutile (110) surface was studied by ATR-FTIR spectroscopy. The spectra indicated that there was only one type of adsorbed species, and that formate and acetate were adsorbed in a similar manner. On the basis of the measured $\nu_{\text{as}}(\text{COO}) - \nu_{\text{s}}(\text{COO})$ splitting ($\Delta\nu_{\text{as-s}}$) of 191 and 87 cm⁻¹, for formate and acetate, respectively, the monodentate (ester type) binding mode could be excluded. Ab initio calculations at the Hartree–Fock level showed that for pentacoordinated Ti^{IV}, present in the (110) surface, the chelating bidentate binding mode is unstable with respect to the rearrangement to the monodentate or the bridging bidentate mode. The computed vibrational frequencies of formate and acetate adsorbed in a bridging bidentate mode onto Ti clusters with 2–5 Ti centers, representing the (110) surface, agreed with experiment and thus showed that this methodology can be used for the determination of the structures of adsorbates on, for example, metal oxide surfaces in contact with aqueous solutions.

Introduction

The determination of the structures of organic compounds adsorbed on surfaces in contact with water or other liquids is important in several systems. Our study is motivated by similar issues in three areas, (i) surface reactions in the environment, (ii) application of mineral particles and semiconductors to pollutant degradation and (iii) photoelectrochemical solar energy conversion. In the environment, adsorption and subsequent thermal or photochemical reactions on mineral surfaces often represent a significant degradation pathway for compounds which are resistant to biodegradation. In advanced oxidation processes for water and air purification, TiO₂ is widely used as a photocatalyst.^{1–5} The adsorption of organic pollutants to the TiO₂ surface has been shown to influence the efficiency of degradation.^{6,7} In the dye-sensitized TiO₂ solar cells developed by Grätzel,^{8–11} the mode of adsorption of the dyes is of crucial importance for the electron injection efficiency and the photoelectrochemical stability of adsorbed dyes.^{8–14} In each of these systems, the interaction of organic molecules with the TiO₂ surface is one of the determining factors in the efficiency of the system. As a result, the surface properties of TiO₂ as well as the adsorption and subsequent surface reactivity of organic molecules on the TiO₂ surface have been extensively studied with various spectroscopic and diffraction methods.

Among various spectroscopic methods, infrared (IR) spectroscopy has been widely utilized to study the structures of small organic molecules adsorbed to surfaces^{15–17} and to follow reaction mechanisms on surfaces.¹⁵ IR spectroscopy is noninvasive, highly sensitive, and sensitive to small structural changes.

Most studies have been conducted in high vacuum environments and/or with dry surfaces,^{18–20} employing self-supporting wafers, dry powders, or single-crystal oxide samples. Due to the strong absorption of IR radiation by water, IR studies of aqueous systems have been limited. With the development of Attenuated Total Reflection (ATR) techniques and high signal-to-noise Fourier Transform Infrared (FTIR) instruments, IR studies of mineral particles in the presence of water have become possible.²¹ ATR-FTIR conveniently achieves the short path lengths and the signal-to-noise required for the subtraction of the water background and for infrared characterization of species on TiO₂ surfaces in the presence of water.^{22–27}

An important class of compounds that show strong and specific interactions with aqueous mineral surfaces are carboxylic and polycarboxylic acids. Carboxylic groups are ubiquitous in natural compounds and pollutants. For the use as sensitizers in photoelectrochemical cells, known dyes are often derivatized with carboxylic acid groups to achieve the binding to TiO₂ surfaces.²⁸ To study the interactions of carboxylic groups with IR spectroscopy and ab initio calculations, we have chosen formate and acetate as the two simplest carboxylic acids.

There are three possible structures (Figure 1) of carboxylate adsorbed on to a TiO₂ surface: in the first, denoted as the η^2 -(RCOO)Ti structure (R = H or CH₃), carboxylate is bound to one Ti^{IV} center in a chelating bidentate mode (Figure 1a). Carboxylate could also be bound to one Ti^{IV} in a monodentate ('ester type') mode, the η^1 -(RCOO)Ti structure (Figure 1b). Finally, the carboxyl group could bind with each of its oxygen atoms to a Ti^{IV} center of the surface yielding the μ -(RCOO)Ti₂ structure (Figure 1c). The Ti–Ti distance of the μ -(RCOO)Ti₂ fragment depends on the exposed surface of TiO₂; for example, it is 2.96 Å for rutile (110)²⁹ and 3.785 Å for anatase (101).³⁰ These two Ti–Ti distances are quite different because in the

* Corresponding authors. E-mail: francois.rotzinger@epfl.ch (F.P.R.); stephan.hug@eawag.ch (S.J.H.).

[†] Ecole Polytechnique Fédérale.

[‡] Swiss Federal Institute for Environmental Science and Technology.

[§] Laboratory of Crystallography, Swiss Federal Institute of Technology.

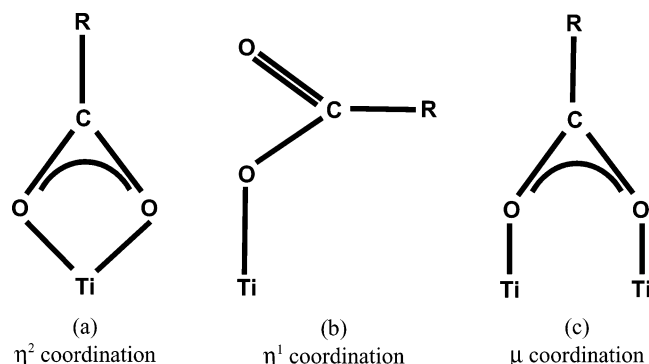


Figure 1. Binding modes of RCOO[−] (R = H or CH₃).

rutile surface, the Ti atoms are bridged by two oxygens, whereas in anatase there is one nearly linear bridging oxygen.

Current evidence indicates that formate^{19,31–36} and acetate^{20,36–39} bind in a bridging bidentate mode (Figure 1c) on the (110) surface of rutile (Figure 2) under high vacuum conditions, whereby the proton of the acid is transferred to the basic oxygen sites.^{32,40–42} Each of these oxygens is bound to two six-coordinated Ti^{IV} centers (Figure 2). Quantum chemical calculations on the interaction of formic acid with models of the rutile TiO₂ (110) surface also predict a bridging bidentate structure.^{40–42}

In this study, the adsorption of HCOOH/HCOO[−] and CH₃COOH/CH₃COO[−] from the aqueous phase on the TiO₂ rutile (110) surface was investigated by ATR-FTIR spectroscopy. Spectra were measured as a function of solution concentration and pH, and multicomponent fitting²² was applied to separate spectral contributions from adsorbed and dissolved species. The adsorption of HCOOH from the gasphase to “dry” rutile was also measured for comparison with other studies. The measured IR frequencies do not allow the deduction of the structure of the adsorbed carboxylate in a direct manner. As it will be shown in the Discussion, the structure assignment on the basis of IR frequencies and the rules of Deacon et al.^{43,44} is not unequivocal: the monodentate (η^1) structure can be ruled out, but the η^2 and μ modes cannot be distinguished.

One way of obtaining structural information on the HCOO[−] and CH₃COO[−] adsorption on TiO₂ is to compute the vibrational

frequencies of hypothetical structures with quantum chemical methods and to compare these data with experiment. This requires the knowledge of the structure of the exposed surface, which was mainly rutile (110) as characterized by high-resolution transmission electron microscopy (HRTEM). Various clusters, modeling formate and acetate adsorbed onto the (110) surface were constructed, and their vibrational frequencies were computed using the Hartree–Fock (HF) method.

Experimental Section

Materials. Analytical grade formate, acetate, NaOH, and HCl were obtained from Merck and used as received. Potassium chloride (99%) was obtained from Fluka and used as supplied. Deuterated formate (99 atom % D) was purchased from Aldrich. All solutions were prepared in Nanopure water (Barnstead Nanopure). The rutile TiO₂ was a gift from Sachtleben.

Characterization of the TiO₂ Surface. The high-resolution transmission electron microscopy (HRTEM) measurements were performed using a Philips CM 30 ST instrument.

Fourier Transform Infrared (FTIR) Measurements. FTIR spectra were recorded on a BioRad FTS45 instrument equipped with a linearized mercury cadmium telluride (MCT) detector and a Specac horizontal attenuated total reflection (ATR) unit with a trapezoidal ZnSe or Ge ATR crystal. The larger horizontal upper probe face of the crystal measures 10 × 72 mm, while the smaller face is 10 × 62 mm. The crystals are 6 mm thick and the trapezoidal angle is 45°, resulting in 5 internal reflections on the upper probe face. Further characterization of the optical properties of the ATR set up, including equivalent path lengths, were reported by Hug et al.²²

The upper surface of the ATR crystal was coated with 1–3 μ m thick TiO₂ layers by application of 20 or 50 μ L of an aqueous suspension (20 mg/mL) of the oxide, followed by air-drying. The layers were subsequently cleaned by soaking in 0.1–1 mM NaOH (pH 9–11) typically between 15 and 30 min. This procedure desorbs residual anions present in the TiO₂ preparations.

A background spectrum was taken with the layer in contact with 100 mL of an aqueous 10 mM KCl background electrolyte solution at the same pH of the subsequent measurements. Small volumes of a concentrated stock solution of formate or acetate

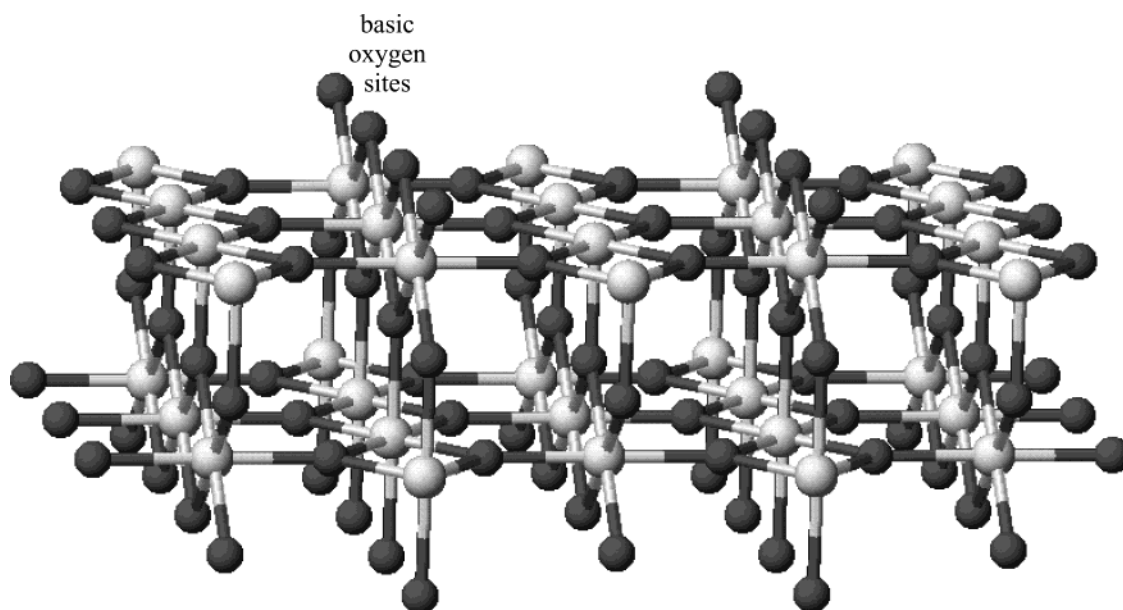
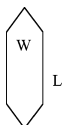


Figure 2. Perspective view of the TiO₂ rutile (110) surface (Ti: gray-scale, O: black).

TABLE 1: Morphological Parameters of the Rutile Nanocrystals

Shape	Morphology	Content in powder	Sizes L, W (nm)	L/W ^a (av)	Mostly exposed faces ^b	Other exposed faces	Termination of crystallites (T, %, approximately)
	Rodlike	100%	40–80 3–5	15	(110)	(101)	T{110}=98

^a L/W is the length/width ratio for an “average” nanocrystallite of given shape. ^b It is difficult to distinguish other exposed faces of nanocrystallites of this shape.

TABLE 2: Calculated Vibrational Frequencies of μ -(HCOO)_{1/2}Ti₂ Clusters Modeling the Rutile (110) Surface

	modes, ^a cm ⁻¹						d(Ti–O), ^b Å	d(Ti–Ti), ^c Å	$\Delta\nu_{as-s}$, cm ⁻¹
	δ (OCO)	π (H–COO)	ν_s (COO)	δ (HCO)	ν_{as} (COO)	ν (CH)			
μ -(HCOO)Ti ₂ O ₂ F ₆ ³⁻	778 (770)	1066 (915)	1375 (1354)	1395 (1031)	1673 (1663)	2633 (1935)	2.264	2.861	298 (309)
μ -(HCOO)Ti ₃ O ₂ F ₁₀ ³⁻	775 (768)	1068 (915)	1369 (1344)	1397 (1034)	1638 (1627)	2746 (2023)	2.184	2.792	269 (283)
μ -(HCOO)Ti ₃ O ₂ F ₁₀ ^{3-d}	775	1069	1369	1397	1636	2751	2.179	2.792	267
μ -(HCOO)Ti ₃ (OH) ₂ F ₁₀ ^{-e}	765 (758)	1084 (922)	1388 (1357)	1379 (1024)	1599 (1587)	2954 (2188)	2.042	3.190	211 (230)
μ -(HCOO)Ti ₃ F ₁₂ ^{-f}	772 (765)	1083 (921)	1385 (1353)	1377 (1023)	1594 (1582)	2960 (2193)	2.051	3.212	209 (229)
μ -(HCOO)Ti ₃ O ₂ F ₈ (OH) ₂ ^{-g}	769 (761)	1080 (920)	1380 (1349)	1377 (1023)	1596 (1583)	2936 (2174)	2.053	2.832	216 (234)
μ -(HCOO)Ti ₃ O ₂ F ₁₀ ·(H ₂ O) ₂ ^{3-h}	778 (770)	1071 (917)	1369 (1343)	1399 (1036)	1626 (1615)	2784 (2053)	2.202	2.782	257 (272)
μ -(HCOO)Ti ₃ (OH) ₂ F ₁₀ ·(H ₂ O) ₂ ^{-e,h}	767 (760)	1083 (921)	1386 (1354)	1381 (1026)	1590 (1578)	2963 (2196)	2.052	3.183	204 (224)
μ -(HCOO)Ti ₅ O ₄ F ₁₆ ^{5-d}	778 (770)	1064 (914)	1371 (1351)	1395 (1030)	1674 (1664)	2590 (1901)	2.283	2.855	303 (313)
μ -(HCOO)Ti ₅ O ₂ F ₂₀ ^{5-d}	775 (768)	1062 (908)	1370 (1342)	1385 (1028)	1593 (1580)	2883 (2129)	2.071	2.890	223 (238)
μ -(HCOO) ₂ Ti ₂ O ₂ F ₄ ²⁻	766 (759), 776 (769)	1071 (917), 1072 (918)	1395 (1336), 1396 (1341)	1363 (1033), 1368 (1034)	1605 (1592), 1629 (1617)	2806 (2070), 2809 (2072)	2.152	2.775	210 (256) 233 (276)
μ -(HCOO) ₂ Ti ₂ F ₆ ^f	756 (748), 783 (777)	1083 (919), 1083 (921)	1368 (1335), 1375 (1342)	1363 (1016), 1369 (1018)	1528 (1511), 1589 (1576)	2997 (2222), 2997 (2223)	2.013	3.166	160 (176) 214 (234)

^a In parentheses: frequencies for the corresponding DCOO⁻ compound. ^b Ti–OOCH bonds. ^c Ti–Ti distance in the Ti₂O₂ unit. ^d Smaller basis set, see ‘Computational Details’. ^e μ -O₂ replaced by μ -(OH)₂. ^f μ -O₂ replaced by μ -F₂. ^g 3 imaginary modes (see text). ^h H-bonding included: the two H₂O are H-bonded to HCOO⁻ and F⁻.

TABLE 3: Calculated Vibrational Frequencies of η^1 and η^2 Bound Acetate, and μ -(CH₃COO)Ti₂ Clusters Modeling the Rutile (110) Surface

	modes, cm ⁻¹						d(Ti–O), ^a Å	d(Ti–Ti), ^b Å	$\Delta\nu_{as-s}$, cm ⁻¹
	δ (OCO)	ν (CC)	δ_s (CH ₃)	δ_{as} (CH ₃)	ν_s (COO)	ν_{as} (COO)			
η^2 -(CH ₃ COO)TiF ₄ ⁻	684	940	1354	1429, 1443	1499	1577	2.172		79
η^2 -(CH ₃ COO)TiF ₄ ·(H ₂ O) ₂ ⁻	685	946	1359	1426, 1442	1504	1563	2.166		58
η^2 -(CH ₃ COO)TiF ₅ ^{2-c}	643	901	1325	1439, 1452	1436	1671	2.597		236
η^1 -(CH ₃ COO)TiF ₅ ²⁻	638	910	1326	1441, 1445	1405	1673	2.073		267
η^1 -(CH ₃ COO)TiF ₅ ·H ₂ O ²⁻	640	916	1331	1440, 1445	1413	1660	2.068		247
μ -(CH ₃ COO)Ti ₃ O ₂ F ₁₀ ³⁻	666	911	1332	1437, 1452	1430	1618	2.175	2.790	188
μ -(CH ₃ COO)Ti ₃ O ₂ F ₁₀ ·(H ₂ O) ₂ ^{3-d}	668	916	1341	1435, 1457	1436	1603	2.189	2.778	168
μ -(CH ₃ COO)Ti ₃ O ₂ F ₁₀ ·(H ₂ O) ₂ ^{3-d,e}	669	915	1341	1434, 1456	1435	1603	2.189, 2.191	2.780	168
μ -(CH ₃ COO)Ti ₃ (OH) ₂ F ₁₀ ^{-f}	653	935	1362	1425, 1439	1482	1566	2.028	3.183	85
μ -(CH ₃ COO)Ti ₃ (OH) ₂ F ₁₀ ·(H ₂ O) ₂ ^{-d,f}	649	935	1366	1423, 1446	1483	1553	2.029	3.173	69
μ -(CH ₃ COO)Ti ₅ O ₂ F ₂₀ ^{5-g}	688	928	1329	1433, 1440	1462	1569	2.065, 2.052	2.889	108

^a Ti–OOCCH₃ bonds. ^b Ti–Ti distance in the Ti₂O₂ unit. ^c Saddlepoint with one imaginary frequency. ^d H-bonding included: the two H₂O are H-bonded to CH₃COO⁻ and F⁻. ^e Isomer with C₁ symmetry. It is slightly more stable (by 0.8 kJ/mol) than the above isomer with C_s symmetry. ^f μ -O₂ replaced by μ -(OH)₂. ^g Smaller basis set, see ‘Computational Details’.

were then added to achieve the total concentrations cited in the figures. In the experiments with pH > 5, purging with high purity N₂ (g) was used to reduce the influence of dissolved carbonates. The spectra at each concentration and pH were then obtained by averaging 1000 scans (4 cm⁻¹ resolution) against the appropriate background spectrum.

The pH of the solution above the TiO₂ layer was controlled and monitored by an Intel 286 based PC with a home-written BASIC program. A Black Star Model 2308 I/O Interface provided the link between the computer and a Metrohm Model 632 pH meter and two automated burets (Metrohm Model 665 Dosimats) containing 0.2 M NaOH(aq) and HCl(aq). The FTIR instrument was controlled by a SPC3200 data station and final data analysis was performed on a PC using Matlab (The MathWorks, Inc, Natick, MA 01760).

Computational Details. All MO calculations have been performed on Cray T3D, HP 9000/C200, HP 9000/735, and Dell Precision 330 computers using the GAMESS⁴⁵ programs.

The basis sets of Stevens, Basch, Krauss and Jasien⁴⁶ were used for titanium, where the 1s, 2s and 2p shells are represented by relativistic effective core potentials, the 3s, 3p, 4s, 4p shells have double- ζ and the 3d triple- ζ quality. For C, O, F and H 6-31G(d) basis sets^{47,48} were used ($\alpha_{3d} = 0.80, 1.20$ and 1.40 ,⁴⁹ respectively). In one case (third entry in Table 2), the polarization functions were omitted on all *terminal* F atoms: geometry and frequencies changed very slightly, and this shows that the smaller basis set is adequate for the large clusters, such as μ -(HCOO)Ti₅O₄F₁₆⁵⁻, μ -(HCOO)Ti₅O₂F₂₀⁵⁻, and μ -(CH₃COO)-Ti₅O₂F₂₀⁵⁻ (Tables 2 and 3).

For every compound reported in Tables S1–S3 and 2–3, a geometry optimization was performed at the Hartree–Fock level for the free ions (in the gas phase). The Hessians were calculated analytically, or numerically⁵³ using the double-difference method, and projected to eliminate rotational and translational contaminants.⁵⁴ No corrections for anharmonicity were made, and all calculated frequencies were scaled by a factor of 0.89. The

geometries correspond to local minima and do not exhibit imaginary frequencies apart from the exceptions mentioned in the text.

The acetate clusters were more difficult to compute because an imaginary frequency describing the rotation of the methyl group was obtained when the geometries were computed with the default convergence criterium (opttol = 1×10^{-4} hartrees/bohr). The imaginary frequency disappeared with more stringent criteria (opttol = 2×10^{-5} hartrees/bohr, vibsiz = 0.003 or 0.005 bohr instead of 0.01 bohr, SCF convergence criterium: 2×10^{-6} instead of 1×10^{-5}). However, it should be noted that the frequencies of interest were not affected by the presence of the imaginary mode.

Results

The characterization of the relevant surfaces of TiO₂ is presented in the first section. The next two sections describe the ATR-FTIR measurements of the adsorption of the carboxylic acids and their anions on TiO₂ layers. Then, the reliability of the computational method is demonstrated for HCOOH in the gas phase, and the vibrational frequencies of various clusters representing the η^2 and η^1 coordination of formate are given. For the μ coordination, clusters representing the (110) rutile surface are systematically improved, whereby the calculated frequencies approach the experimental data. Finally, the frequencies of acetate, computed for the three possible binding modes (Figure 1) on the basis of the best formate clusters are presented. Based on these data, the structure of formate and acetate adsorbed onto the rutile (110) surface from aqueous solution was determined.

Characterization of the TiO₂ Powder. The morphology of the rutile nanocrystals is shown by their HRTEM patterns (Figure 3). The length and thickness of the particles vary within the range of roughly 40–80 nm and 3–5 nm respectively (Table 1). The interplanar separations, which could be distinguished on HRTEM patterns, show that mostly the (110) faces are exposed. Furthermore, the separations corresponding to (101) faces could be determined. A very rough estimation using the HRTEM images shows that more than 95–98% of the exposed faces of the rutile nanocrystals are formed by (110) faces. The interplane separations corresponding to the (101) faces could also be seen; they contribute to the termination of nanocrystals from the basal sides.

ATR-FTIR Measurements. The infrared (IR) spectra of 1 M aqueous formate and formic acid, measured with the uncoated ATR crystal, are shown in Figure 4. For easier comparison, the spectra have been normalized to a maximum amplitude of one and are offset from each other. (The original amplitudes are indicated in the figure). The peak positions for the antisymmetric $\nu_{\text{as}}(\text{COO})$ vibration at 1580 cm^{-1} and the symmetric $\nu_{\text{s}}(\text{COO})$ vibration at 1350 cm^{-1} agree with those given for aqueous formate by Nakamoto.⁵⁵ The energy difference between $\nu_{\text{as}}(\text{COO})$ and $\nu_{\text{s}}(\text{COO})$, $\Delta\nu_{\text{as-s}}$, is 230 cm^{-1} . The spectrum of formic acid (pH 2.2) shows an absorbance at 1719 cm^{-1} , typical of C=O vibrations and an absorbance peak at 1211 cm^{-1} typical of a C–OH vibration. Water strongly absorbs at 1630 cm^{-1} , and previous research has shown that changes in pH, ionic strength etc., can influence the intensity of the water band observed in ATR experiments. Thus, spectral changes in this wavenumber region are difficult to interpret due to this interference by the changing water band.

Figure 5 shows ATR spectra measured with the ATR-crystal coated with a layer of rutile TiO₂ particles in contact with 250 μM to 30 mM aqueous formate at pH 5.0. The spectra contain

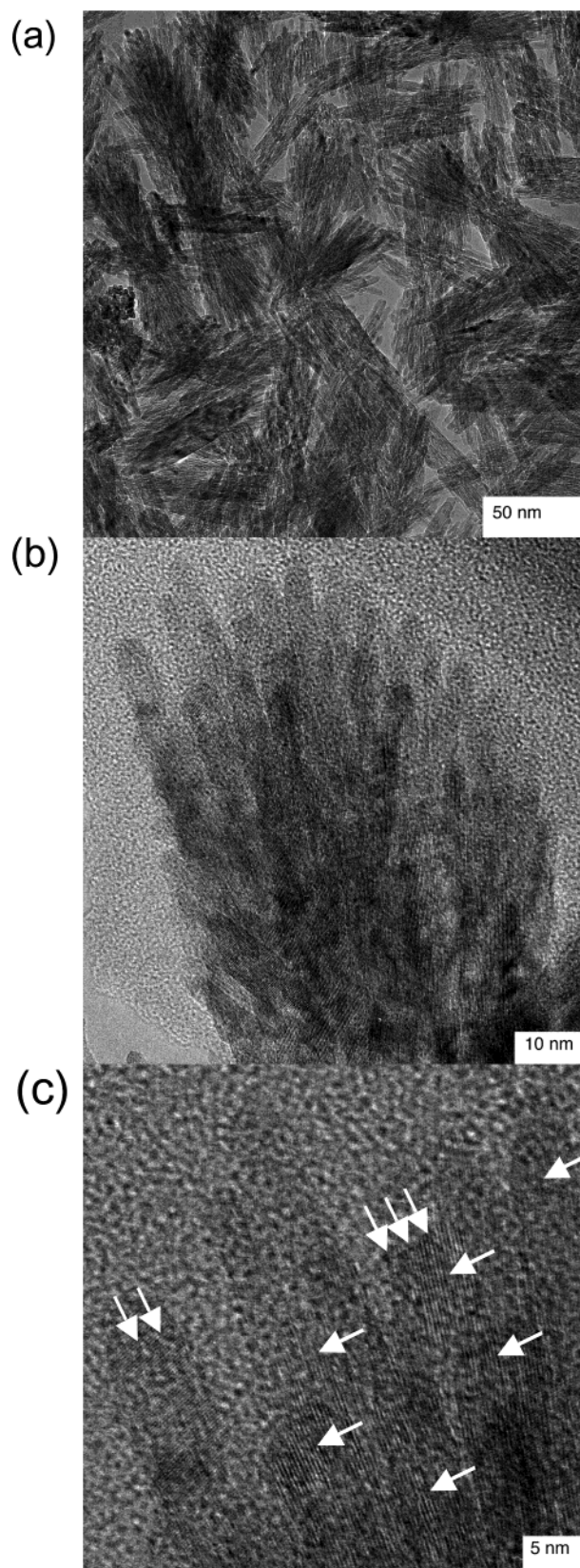


Figure 3. HRTEM micrographs of rutile particles. (a) "Bundles" of rodlike rutile nanocrystals; (b) higher magnification: the nanocrystals are terminated by the mostly exposed (110) faces. The average relation length/width (L/W) is ca. 15. (c) The (110) fringes ($d = 3.25 \text{ \AA}$) are shown with arrows, the (101) fringes ($d = 2.49 \text{ \AA}$) are shown with double arrows, the fringes intersection, allowing to determine the dihedral angles between (110) and (101) faces (ca. 116.5°) is shown by triple arrows. The symmetrical packing planes (110) are parallel to anions sheets in the rutile structure.

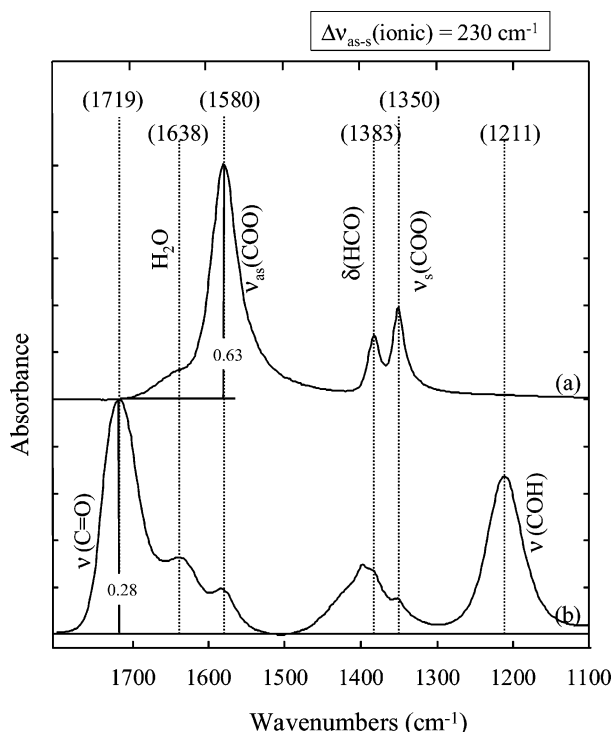


Figure 4. (a) Normalized ATR-FTIR spectrum of 1 M formate (aqueous) at pH 6.3, no added electrolyte. (b) Normalized ATR-FTIR spectrum of 1 M formic acid (aqueous) at pH 2.

spectral contributions from both dissolved and adsorbed formate. These contributions can be separated into a spectral component originating from the aqueous (dissolved) formate that increases linearly with the aqueous concentration and a component originating from adsorbed formate which is described by an adsorption isotherm, typically a Langmuir isotherm. The mathematical procedure, which employs singular value decomposition (SVD) and multicomponent fitting, is described in details elsewhere.²² The separated linear and Langmuir spectral components are shown in the top part of the figure, together with their relative contributions in the inset. The Langmuir adsorption constant given in the figure inset is a conditional, fitted equilibrium constant for the adsorption of formate at pH 5.0. Also shown are the residuals (differences between original spectra and the spectra fitted with the linear and Langmuir components). Residuals are shown offset from each other directly above the spectra and show that within experimental error, all spectra are well reproduced with the two spectral components. Comparison of the spectra of the adsorbed component with the spectrum of aqueous formate (Figure 4) reveals a new peak at 1540 cm^{-1} and a shoulder appearing on the low energy side of the 1351 cm^{-1} peak. We assign the peak at 1540 cm^{-1} to the $\nu_{\text{as}}(\text{COO})$ vibration which has been shifted by 40 cm^{-1} to lower energy by interaction with the TiO_2 surface. This reduces the separation between $\nu_{\text{as}}(\text{COO})$ and $\nu_{\text{s}}(\text{COO})$, $\Delta\nu_{\text{as-s}}$, from 230 to 191 cm^{-1} . In the case of formate, where the $\nu_{\text{as}}(\text{COO})$ vibration is clearly shifted upon adsorption while the $\nu_{\text{s}}(\text{COO})$ vibration remains nearly unchanged, the spectral changes can also be determined directly from the original (nondeconvoluted) spectra, from which a $\Delta\nu_{\text{as-s}} = 192 \text{ cm}^{-1}$ is obtained.

To be able to make definitive assignments for the closely situated $\delta(\text{HCO})$ and $\nu_{\text{s}}(\text{COO})$ bands in the 1350–1400 cm^{-1} region, we conducted analogous experiments with deuterated formate. Because the $\delta(\text{DCO})$ vibration of d-formate is shifted to energies far below those of the $\nu_{\text{s}}(\text{COO})$ vibration, shifts in

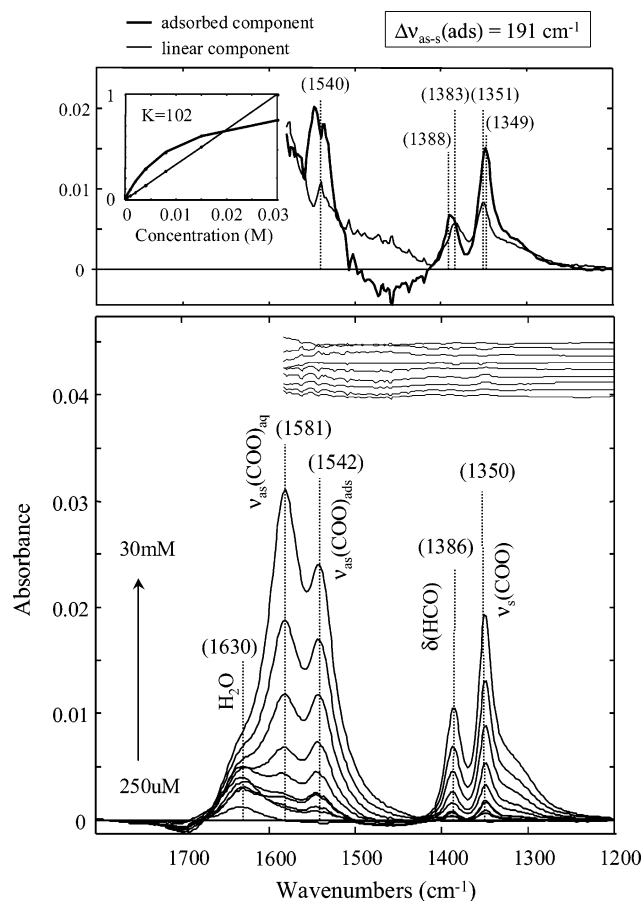


Figure 5. ATR-FTIR spectra of aqueous solutions of formate in contact with a layer of rutile TiO_2 (1.0 mg applied) at pH 5.0. The concentrations of formate in solution are: 0, 0.25, 0.5, 1, 1, 2, 4, 8, 15, and 30 mM. The spectra of the adsorbed and linear components, obtained as described in the text, are shown above the experimental spectra. The inset graph shows the contributions of each of these components as a function of solution concentration.

either of these peaks are more easily determined for the deuterated formate. The infrared spectra of d-formate in aqueous solution and adsorbed to rutile are shown in Figure 6. The δ -(DCO) vibration is observed at 1024 cm^{-1} in the aqueous and at 1030 cm^{-1} in the adsorbed d-formate. Similar to nondeuterated formate, adsorption of d-formate on rutile leads to a shift of the $\nu_{\text{as}}(\text{COO})$ from 1572 cm^{-1} by 38 cm^{-1} to 1534 cm^{-1} . $\Delta\nu_{\text{as-s}}$ in d-formate decreases from 246 to 212 cm^{-1} upon adsorption. Upon deuteration of formate, $(\Delta\nu_{\text{as-s}})_{\text{ads}}$ increases by 21 cm^{-1} .

The pH dependence with 5 mM formate on rutile is depicted in Figure 7. The solution pH was controlled as described in the Experimental Section. Figure 7 shows the targeted and measured pH and the amount of adsorbed formate (empty circles), obtained by integration of the surface specific $\nu_{\text{as}}(\text{COO})$ band at 1530–1560 cm^{-1} . The corresponding spectra are shown in Figure 8, where it can be seen that the formate peak positions shift only slightly over the pH range from 3 to 6. (Changes at 1630 cm^{-1} due to H_2O are caused by changes of surface hydration or protonation). At pH 9, formate does not adsorb and only the contribution from the aqueous formate is seen and agrees well with the spectra of aqueous formate measured without a TiO_2 layer shown in Figure 4. At lower pH, the contribution from adsorbed formate becomes dominant, with the new $\nu_{\text{as}}(\text{COO})$ band at 1541 cm^{-1} , close to the 1540 cm^{-1} in Figure 5. Even at pH 3, no evidence for adsorbed formic

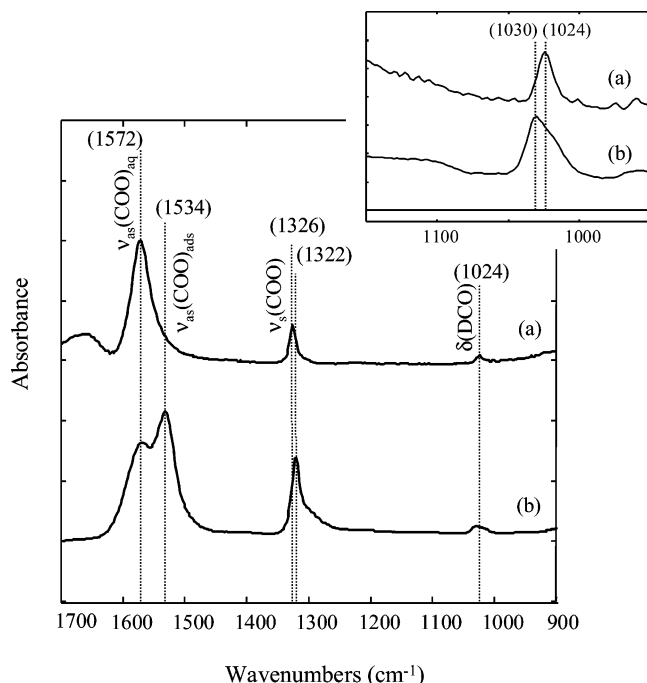


Figure 6. (a) Normalized ATR-FTIR spectrum of 10 mM d-formate (aqueous) at pH 5.0, no added electrolyte. (b) Normalized ATR-FTIR spectrum of 5 mM d-formate at pH 4.5 in contact with a layer of rutile (0.4 mg applied).

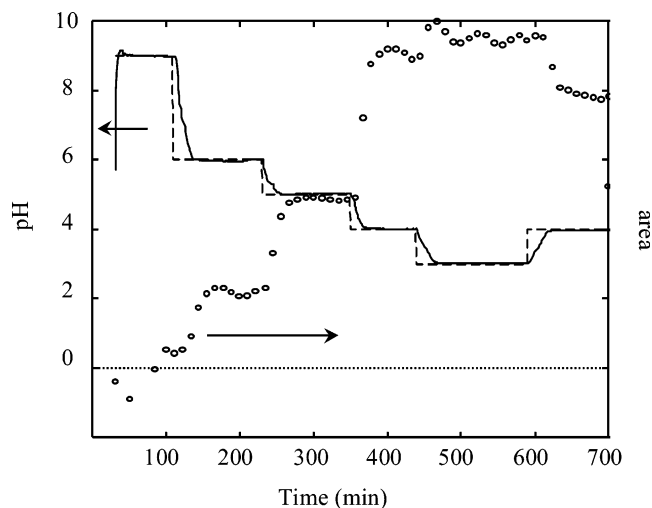


Figure 7. pH dependence of the adsorption of 5 mM formate on a rutile TiO₂ layer. Solid line: measured pH; dashed line: targeted pH. Circles: relative amount of adsorbed formate obtained by integrating the area between 1530 and 1560 cm⁻¹.

acid is observed, with only a weak signal from aqueous formic acid at 1720 cm⁻¹.

Previous studies have measured formate adsorption from the gas phase to nominally dry surfaces (at ambient humidities mineral surfaces are always covered with several layers of adsorbed water). Formic acid adsorbed from the gas phase has been reported to dissociate to formate on nominally dry layers of both rutile and anatase (acetate on anatase,¹⁶ formate on rutile⁵⁶). Figure 9 shows the spectra of rutile layers that have been "dried" by a stream of flowing nitrogen and subsequently been exposed to N₂ in equilibrium with formic acid. Contributions from both formate (1355, 1377, and 1533 cm⁻¹) and physisorbed formic acid (1204 and 1716 cm⁻¹) are observed in these spectra. The peaks due to formate are very similar to those of formate adsorbed in the presence of aqueous phase and only

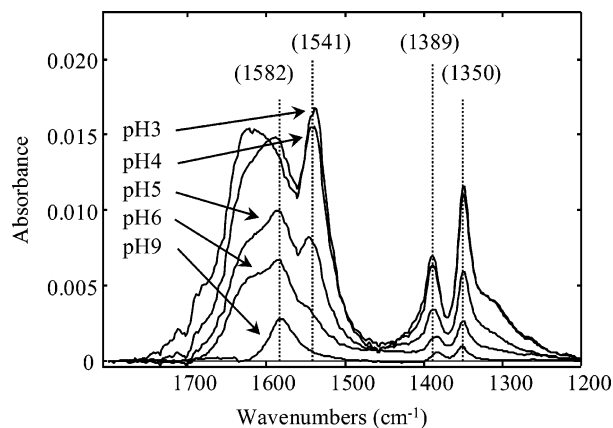


Figure 8. ATR-FTIR spectra of 5 mM formate in contact with a rutile layer at the indicated pH values.

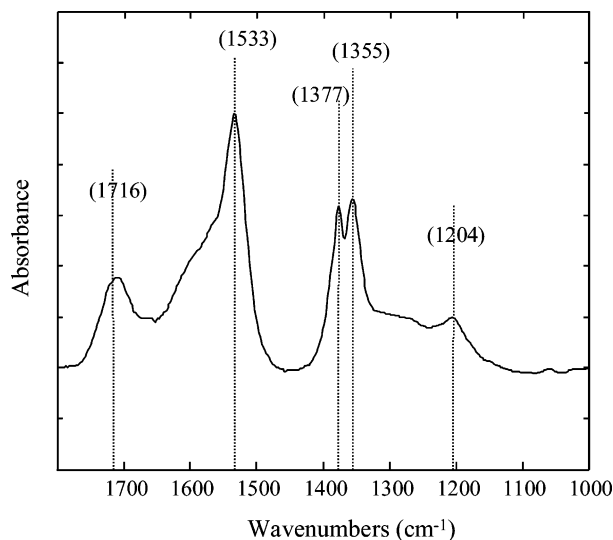


Figure 9. Normalized adsorption of formic acid from the gas phase on rutile TiO₂ layers.

slightly shifted (≤ 11 cm⁻¹) from their respective values on these surfaces in aqueous solution.

Figure 10 shows normalized (maximum amplitude of 1.0) spectra of 250 mM aqueous acetate and acetic acid at (a) pH 8.0 and at (b) pH 2.1. These spectra are similar to the spectra of formate and formic acid shown in Figure 4, but with different peak positions and intensities. In acetate, ν_s(COO) has much more intensity than the δ(CH₃) vibration, while in formate, the intensities of ν_s(COO) and δ(HCO) are almost equal, and the positions in energy are switched. These differences are due to the much stronger coupling of ν_s(COO) and δ(HCO) in formate than the coupling between ν_s(COO) and δ(CH₃) in acetate.

Figure 11 shows spectra with a layer of rutile TiO₂ particles in contact with 0 μM to 25 mM aqueous acetate. As was the case with formate, these spectra contain contributions from dissolved and adsorbed acetate. The decomposed linear and Langmuir spectral components are shown in the top part of the figure. The comparison of dissolved and adsorbed acetate reveals a shift of ν_{as}(COO) from 1552 to 1513 cm⁻¹, of ν_s(COO) from 1415 to 1426 cm⁻¹ and of δ(CH₃) 1348 to 1352 cm⁻¹. For acetate, Δν_{as-s} decreases from 137 to 87 cm⁻¹ upon adsorption. From the nondeconvoluted spectra (Figure 11), a slightly higher Δν_{as-s} of 90 cm⁻¹ is obtained.

The pH dependence of acetate adsorption on the rutile layer is shown in Figure 12. The adsorbed amount of acetate was obtained by integration of the 1512 cm⁻¹ peak. In contrast to

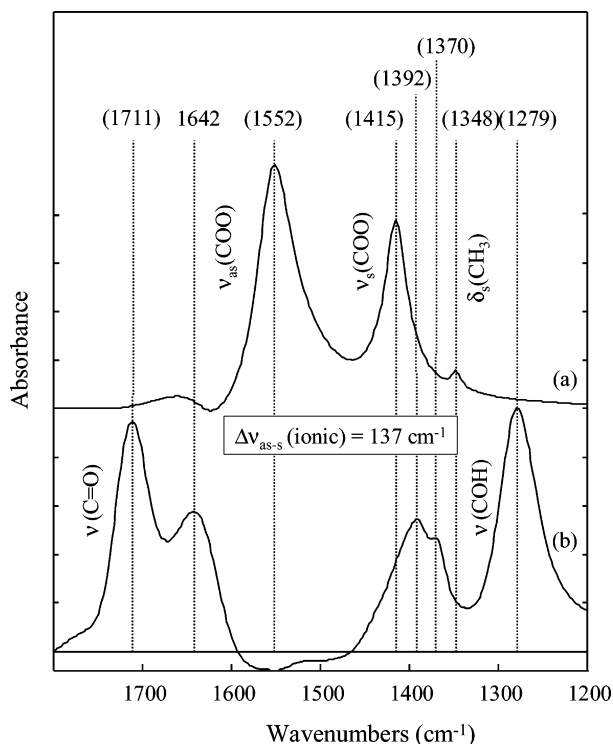


Figure 10. (a) Normalized ATR-FTIR spectrum of 250 mM acetate (aqueous) at pH 8.0, 10 mM KCl electrolyte. (b) Normalized spectrum of 250 mM acetic acid (aqueous) at pH 2.1, 10 mM KCl electrolyte.

formate, which reaches a maximum at pH 3.0, the maximum adsorption for acetate is at pH 4.0, with a significant but reversible decrease at pH 3.0. This difference is well explained in the context of the one- or two- pK_a surface complexation model and the different pK_a values of formate (pK_a 3.75) and of acetate (pK_a 4.8).

Possible Structures of Adsorbed Formate and Acetate. The above-described experiments show that only (deprotonated) formate or acetate is adsorbed onto TiO_2 from aqueous solutions. Therefore, on the rutile (110) surface (Figure 2) the three structures of $RCOO^-$ ($R = H$ or CH_3) shown in the Introduction (Figure 1) will be considered. In the following section, the vibrational frequencies of the formate and acetate ions, calculated on the basis of Ti^{IV} clusters representing the (110) surface and the three possible binding modes (Figure 1), are described.

Quantum Chemical Computation of the Vibrational Frequencies. (a) **Model of Adsorbed Species on the Rutile Surface.** Frequencies, computed using density functional theory deviate on both sides of the measured values, whereas in general, ab initio self-consistent field (SCF) methods overestimate the frequencies by a *constant* factor. Hence, by applying a scaling factor, typically 0.89, which was used in the present study, small deviations are obtained. This is the reason we chose to compute the frequencies using Hartree–Fock (HF) on the basis of TiO_2 clusters representing the rutile (110) surface. The clusters have been constructed by maintaining the coordination number of Ti^{IV} at 6 and therefore, all the clusters are negatively charged. To reduce this charge, which has the tendency to repel the carboxylate anion, other clusters, in which the oxo groups having coordination numbers smaller than 3 were replaced by fluoride, hydroxide or water, have also been investigated. The limitations of this approach will be discussed in the corresponding context. Hydrogen bonding of adsorbed formate and acetate with the solvent was considered for all of the three binding modes (Figure 1). It was modeled with one or two water molecules interacting with the carboxylate ion.

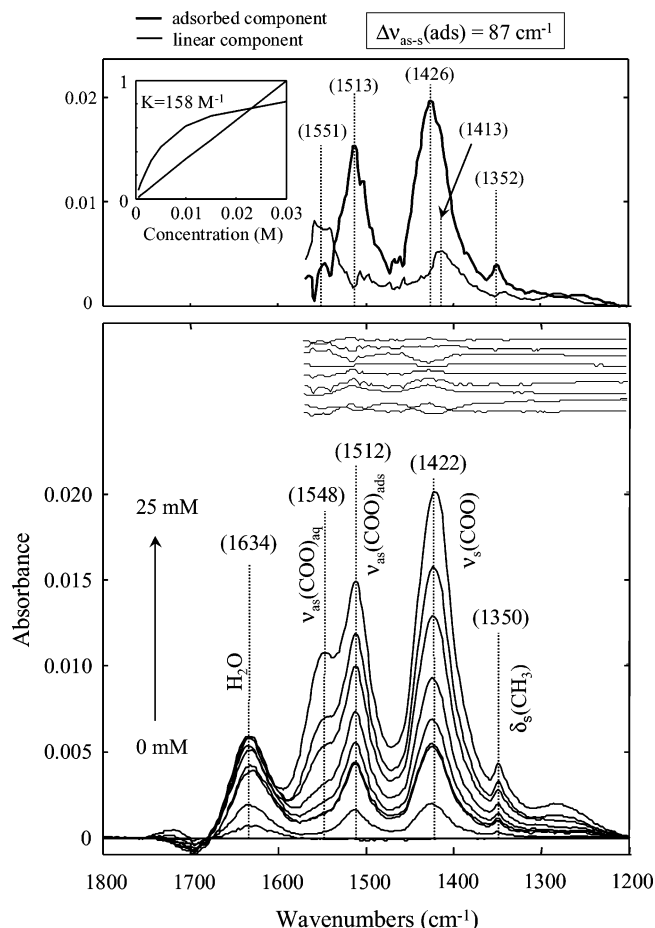


Figure 11. ATR-FTIR spectra of aqueous acetate in contact with a layer of rutile (1.0 mg applied) at pH 5.0. The concentrations of acetate in solution are: 0, 0.5, 1, 2, 3, 5, 10, 15, and 25 mM. The spectra of the adsorbed and linear components, obtained as described in the text, are shown above the experimental spectra.

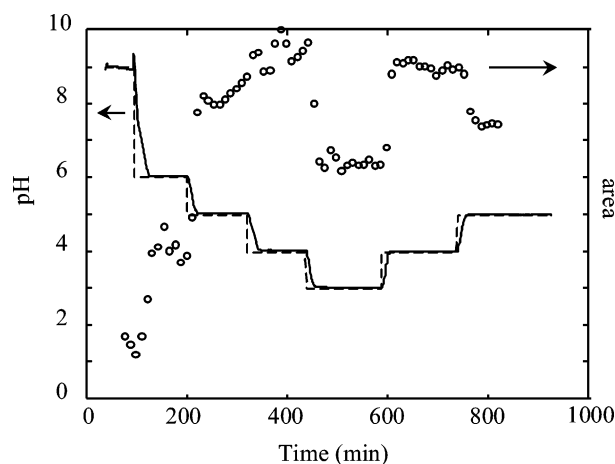


Figure 12. pH dependence of adsorption of 5 mM acetate on a rutile layer. Solid line: measured pH; dashed line: targeted pH. Circles: relative amount of adsorbed formate obtained by integrating the area between 1495 and 1540 cm^{-1} .

(b) **Vibrational Spectrum of *trans*-HCOOH in the Gas Phase and *cis*-HCOOH in a Solid Argon Matrix. Validation of the Model.** The spectrum for the stable *trans* conformer is known,^{50,51} whereas for the *cis* conformer, it has been obtained only recently.⁵² These experimental vibrational spectra are used to assess the reliability of the Hartree–Fock method. The experimental data (Table S1) is compared with the, for small molecules such as HCOOH, low level of calculations, that

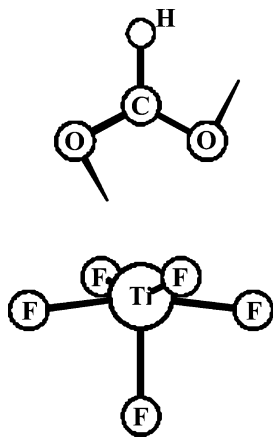


Figure 13. Perspective view and imaginary mode of $\eta^2\text{-(HCOO)TiF}_5^{2-}$, which is the transition state for the rearrangement of $\eta^1\text{-(HCOO)TiF}_5^{2-}$.

however, allows computations of HCOO[−] and CH₃COO[−] bound to clusters with up to 5 Ti^{IV} centers. The calculated scaled frequencies deviate by less than 70 cm^{−1} from the experimental ones, and it will be shown that this precision is sufficient for the interpretation of the present ATR-FTIR spectra.

The calculated and measured frequencies of the $\delta(\text{HCO})$, $\nu_s(\text{COO})$ and $\nu_{as}(\text{COO})$ modes of *trans/cis*-HCOOH, differ by 6/21, 38/12 and 47/48 cm^{−1}, respectively. Only these modes were observed by ATR-FTIR spectroscopy and were thus available for the determination of the structure of HCOO[−] adsorbed onto the rutile (110) surface.

(c) $\eta^2\text{-(HCOO)Ti}$ Structure. The bidentate mononuclear binding mode is represented in Figure 1a, and its structure and vibrational spectrum was investigated on the basis of three model compounds. In the first one, $\eta^2\text{-(HCOO)TiF}_4^-$ (Figure S1a), the coordination number of Ti is 6, and this species with *C*_{2v} symmetry is in a local minimum of the potential energy surface. In contrast, the analogous heptacoordinated $\eta^2\text{-(HCOO)TiF}_5^{2-}$ model compound (Figure 13) is the transition state for the rearrangement of the $\eta^1\text{-(HCOO)TiF}_5^{2-}$ species (Figure S2a). Furthermore, this transition state exhibits two very long Ti–O bonds (Table S2). The imaginary mode (Figure 13) indicates that hepta coordination is unfavorable with respect to hexa coordination, since it describes a rotation of the $\eta^2\text{-(HCOO)}$ ligand to form the $\eta^1\text{-(HCOO)Ti}$ structure (Figure S2a). To make sure that this instability is not due to the 2- charge, computations on *trans*- $\eta^2\text{-(HCOO)Ti(OH}_2\text{)F}_4^-$ have also been performed. This species, in *C*_{2v} symmetry, exhibits also an imaginary mode that describes the out-of-plane bending of H₂O together with the elongation of the Ti–O(H₂) bond. Computations of the corresponding intrinsic reaction coordinate lead to a product resembling $\eta^2\text{-(HCOO)TiF}_4^-$ (Figure S1a). The water ligand dissociates and ends in the second coordination sphere, where it is hydrogen bonded to two fluorides (Figure S3).

The computed frequencies of the three $\eta^2\text{-(HCOO)Ti}$ species are reported in Table S2. The out-of-plane bending of H frequencies, $\pi(\text{H-COO})$, are the same for all 4 structures, and also $\nu_s(\text{COO})$ is quite insensitive to the charge and the coordination number of Ti^{IV}. The frequencies of the corresponding compounds with deuterated formate, DCOO[−], are all shifted to lower energies. For the $\delta(\text{OCO})$, $\nu_s(\text{COO})$, and $\nu_{as}(\text{COO})$ modes, the shifts are small (<40 cm^{−1}), but they are quite large for $\nu(\text{CH})$ (\approx 700 cm^{−1}), $\delta(\text{HCO})$ (\approx 350 cm^{−1}) and $\pi(\text{H-COO})$ (\approx 160 cm^{−1}).

Adsorbed formate in contact with an aqueous solution is expected to be H-bonded. To determine the effect of H-bonding onto the vibrational frequencies, the diaqua adduct of the stable

$\eta^2\text{-(HCOO)TiF}_4^-$ complex, $\eta^2\text{-(HCOO)TiF}_4 \cdot (\text{H}_2\text{O})_2^-$ (Figure S1b), was also investigated. H-bonding alters the $\delta(\text{OCO})$, $\pi(\text{H-COO})$, $\nu_s(\text{COO})$, and $\delta(\text{HCO})$ frequencies by ≤ 4 cm^{−1} (Table S2, first two entries), but $\nu_{as}(\text{COO})$ is lowered by 13 cm^{−1} whereas $\nu(\text{CH})$ is increased by 34 cm^{−1}. The Ti–O bonds change very little. The reduction of $\nu_{as}(\text{COO})$ affects $\Delta\nu_{as-s}$ which is reduced by 14 cm^{−1}.

The present calculations suggest that the chelating bidentate (η^2) coordination mode requires *tetracoordinated* Ti^{IV}, that might exist on edges and corners, but not on surfaces. The most reactive sites of the (110) surface (Figure 2) exhibit *penta-coordinated* Ti^{IV}.

(d) $\eta^1\text{-(HCOO)Ti}$ Structure. In Table S3 are summarized 13 structures of the $\eta^1\text{-(HCOO)TiX}_5^{n-}$ type (see e. g. Figure S2a), where X₅ = F₅, F₄(OH), F₄(OH₂), and F₃(OH₂)₂. The OH[−] and H₂O ligands are in *trans* or *cis* position of the HCOO[−] group. For the *cis* isomers, there are internal H-bonds between HCOO[−] and OH[−] or H₂O.

Interestingly, the in-plane HCO deformation, $\delta(\text{HCO})$, exhibits little sensitivity to H-bonding by *cis* H₂O and lies in the range of 1386–1409 cm^{−1}. The asymmetric C–O stretching mode, $\nu_{as}(\text{COO})$, however, depends strongly on both the charge and H-bonding of the model compound. It spans a range of 100 cm^{−1} from 1657 to 1758 cm^{−1}. Also the symmetric C–O stretching mode, $\nu_s(\text{COO})$, is sensitive to the cluster, with frequencies between 1282 and 1360 cm^{−1}. The $\delta(\text{HCO})$ mode, however, is not only insensitive to H-bonding, but also to the cluster.

In addition to the hexa coordinated clusters, a penta coordinated one, $\eta^1\text{-(HCOO)TiF}_4^-$, is included. Compared with $\eta^1\text{-(HCOO)TiF}_5^{2-}$, where also no H-bonds are present, the $\nu_{as}(\text{COO}) - \nu_s(\text{COO})$ difference is larger, but $\delta(\text{HCO})$ remains in the same range as for the other model compounds.

A calculation with formic acid coordinated to TiF₅[−], $\eta^1\text{-(HCOOH)TiF}_5^-$, was also performed. Apart from the large $\nu_{as}(\text{COO}) - \nu_s(\text{COO})$ splitting, a shift of $\delta(\text{HCO})$ by more than 20 cm^{−1} and one of the out-of-plane H–COO bending, $\pi(\text{H-COO})$, by more than −20 cm^{−1} was obtained. As expected, the Ti–OC(OH)H bond is weak (2.398 Å). Interestingly, for adsorbed d₁-formic acid, DCOOH, the computed $\Delta\nu_{as-s}$ is *smaller* than for HCOOH (Table S3). In contrast, the experimental $\Delta\nu_{as-s}$ is larger for d₁-formic acid.

The replacement of F[−] by OH[−] does not alter the vibrational frequencies significantly. This observation will be exploited in the larger clusters exhibiting the $\mu\text{-(HCOO)Ti}_2$ structure element to save computer time by using F[−] instead of OH[−] (viz. next section). Replacing F[−] *trans* to HCOO[−] by water leads to considerably shorter Ti–OOCH bonds, and $\nu_s(\text{COO})$ shifts to lower energies by 100 cm^{−1}. The substitution of F[−] by OH₂ in *cis* position changes the frequencies very little; the changes arise most likely from H-bonding.

For deuterated formate, the shifts are similar to those found for the $\eta^2\text{-(HCOO)Ti}$ structure.

The influence of H-bonding with the solvent on the frequencies is estimated via two H₂O adducts of the $\eta^1\text{-(HCOO)TiF}_5^{2-}$ cluster (Table S3). In the first $\eta^1\text{-(HCOO)TiF}_5 \cdot \text{H}_2\text{O}^{2-}$ isomer (Figure S2b), each H of H₂O forms one H-bond to each O of HCOO[−]. In the second isomer (Figure S2c), one H of H₂O forms a H-bond to one O of HCOO[−], and the other H forms a H-bond to a *cis* F[−] anion of the cluster. H-bonding shifts $\delta(\text{OCO})$ slightly (by 4 and 9 cm^{−1}) to higher values, $\pi(\text{H-COO})$ remains virtually unaffected, $\nu_s(\text{COO})$ fluctuates by +16 and −6 cm^{−1}, and $\delta(\text{HCO})$ is lowered slightly (by −14 and −3 cm^{−1}). Larger effects are observed on $\nu_{as}(\text{COO})$, which is lowered by −24

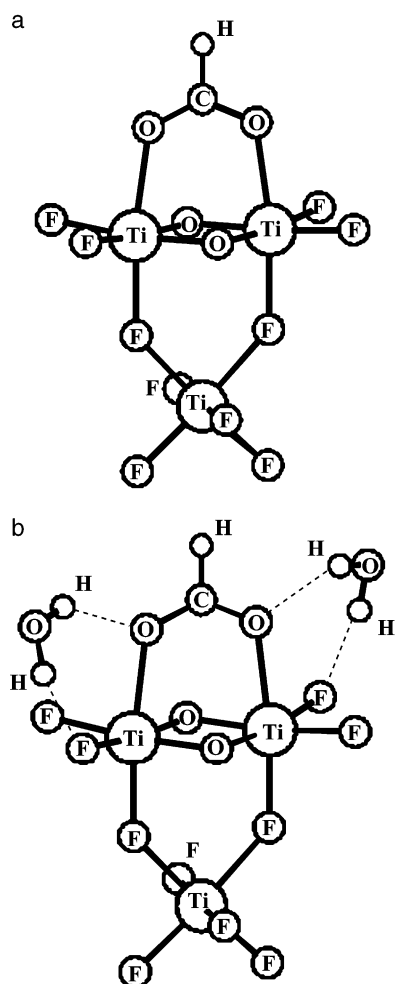


Figure 14. Perspective view of (a) the $\mu\text{-(HCOO)Ti}_3\text{O}_2\text{F}_{10}^{3-}$ cluster and (b) the $\mu\text{-(HCOO)Ti}_3\text{O}_2\text{F}_{10} \cdot (\text{H}_2\text{O})_2^{3-}$ cluster.

and -11 cm^{-1} , and on $\nu(\text{CH})$ which increases by 37 and 21 cm^{-1} . H-bonding lowers $\Delta\nu_{\text{as-s}}$ which, however, remains larger than 320 cm^{-1} .

(e) $\mu\text{-(HCOO)Ti}_2$ Structure. The “active” TiO_2 rutile (110) surface (Figure 2) consists of Ti_2O_2 units and hence, the smallest cluster with this structural element is $\mu\text{-(HCOO)Ti}_2\text{O}_2\text{F}_6^{3-}$ (Figure S4). The two Ti-OCH bonds are relatively long (Table 2) because of the trans effect exerted by the two F^- ligands. This structure is quite distorted, and the Ti-Ti distance is slightly shorter than in the (110) surface. To increase the coordination number of these two trans F^- ligands and to correct the distortion, the cluster was augmented by one TiF_4 unit. This lead to the $\mu\text{-(HCOO)Ti}_3\text{O}_2\text{F}_{10}^{3-}$ cluster (Figure 14a) with a Ti-Ti distance shorter than the experimental value of 2.96 \AA . The charge is the same as that of the previously described Ti_2 cluster, but it is distributed over three Ti centers. This augmentation affects $\nu_{\text{as}}(\text{COO})$ and $\nu(\text{CH})$ considerably: the former diminishes by 35 cm^{-1} and the latter increases by 113 cm^{-1} . It should be noted that for $\mu\text{-(HCOO)Ti}_2\text{O}_2\text{F}_6^{3-}$, $\mu\text{-(HCOO)Ti}_3\text{O}_2\text{F}_{10}^{3-}$, $\mu\text{-(HCOO)Ti}_3\text{O}_2\text{F}_{10} \cdot (\text{H}_2\text{O})_2^{3-}$, and also $\mu\text{-(HCOO)Ti}_5\text{O}_4\text{F}_{16}^{5-}$ and $\mu\text{-(HCOO)Ti}_5\text{O}_2\text{F}_{20}^{5-}$ (see below), $\delta(\text{HCO})$ is greater than $\nu_s(\text{COO})$ by about 20 cm^{-1} .

The oxygen atoms in the (110) surface (Figure 2), belonging to the Ti_2O_2 fragments exhibiting Ti centers with a vacant coordination site, are coordinated to 3 Ti^{IV} ions. Since in the previously described two clusters, these bridging oxygens are bound to two Ti atoms only, another cluster has been constructed in which these two oxygens are protonated to exhibit the

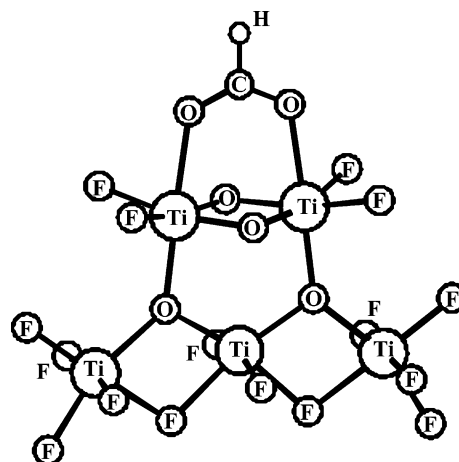


Figure 15. Perspective view of the $\mu\text{-(HCOO)Ti}_5\text{O}_4\text{F}_{16}^{5-}$ cluster (with C_{2v} symmetry).

coordination number of 3. Thereby, the charge is reduced by 2, and the Ti-Ti distance in the Ti_2O_2 fragment increases and becomes considerably larger than the experimental value (Table 2). This modification raises $\pi(\text{H-COO})$ and $\nu_s(\text{COO})$, and lowers $\delta(\text{HCO})$ a little bit (by less than 20 cm^{-1}). The $\nu_{\text{as}}(\text{COO})$ mode decreases (by more than 30 cm^{-1}) and $\nu(\text{CH})$ increases strongly (by about 200 cm^{-1}). A replacement of the $\mu\text{-OH}^-$ bridges by F^- does not alter the frequencies, and this shows that the total charge of the cluster is more important than the coordination number of the $\mu\text{-O}_2$ group. If, in the $\mu\text{-(HCOO)Ti}_3\text{O}_2\text{F}_{10}^{3-}$ cluster, the two axial F^- ligands of the third Ti atom (that is added as a TiF_4 unit) are replaced by water, the charge is the same as that of the above two Ti_3 clusters, and again, the calculated frequencies remain the same. Three imaginary frequencies that describe motions of these two trans water ligands are obtained. They arise from the imposed C_{2v} symmetry and would disappear by lowering of the symmetry. Calculations with a lower symmetry have not been performed because they are quite CPU demanding. Furthermore, the vibrational frequencies involving HCOO^- are unlikely to be affected, since these water ligands are quite distant from the HCOO^- group.

Although the reduction of the charge in the Ti_3 clusters changes the $\nu_s(\text{COO})$ and $\delta(\text{HCO})$ modes by about $+20\text{ cm}^{-1}$ and -20 cm^{-1} , respectively, their order was changed such that in the singly negatively charged clusters, $\nu_s(\text{COO})$ is greater than $\delta(\text{HCO})$. This is opposite to the ATR-FTIR measurements.

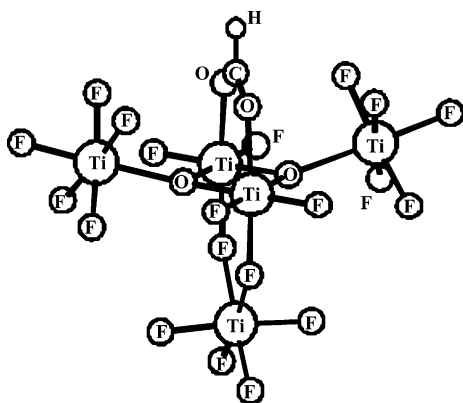
For an improved modeling of the sites trans to HCOO^- , a Ti_5 cluster, $\mu\text{-(HCOO)Ti}_5\text{O}_4\text{F}_{16}^{5-}$, is investigated (Figure 15). It has one negative charge for each Ti atom as in $\mu\text{-(HCOO)Ti}_3\text{O}_2\text{F}_{10}^{3-}$. With the exception of $\nu(\text{CH})$, its calculated vibrational frequencies are the same within a few wavenumbers as those of the smaller clusters. The $\nu(\text{CH})$ frequencies depend most strongly on the cluster, especially on its charge. The more negative the charge, the lower $\nu(\text{CH})$ and the larger its error. Since $\nu(\text{CH})$ is not detectable in the present experiments, its calculated value is not relevant in this context. The calculated $\nu_{\text{as}}(\text{COO})$ mode fluctuates by $\sim 80\text{ cm}^{-1}$ and therefore, its correlation with experimental data has to be done with care.

For a better description of the Ti_2O_2 fragment, two TiF_5^- fragments were added to the bridging oxygens of $\mu\text{-(HCOO)Ti}_3\text{O}_2\text{F}_{10}^{3-}$. In the thus obtained $\mu\text{-(HCOO)Ti}_5\text{O}_2\text{F}_{20}^{5-}$ cluster (Figure 16) with a Ti-Ti distance close to the experimental value (Table 2), the order of the $\nu_s(\text{COO}) - \delta(\text{HCO}) - \nu_{\text{as}}(\text{COO})$ frequencies is correct, but $\nu_{\text{as}}(\text{COO})$ is too high as in all of the other clusters. It should be noted that in the calculations on *trans*- and *cis*- HCOOH (Table S1), $\nu_{\text{as}}(\text{COO})$ was too high

TABLE 4: Selected Calculated Vibrational Frequencies (cm⁻¹) for the Three Pertinent Binding Modes of HCOO⁻, DCOO⁻, and CH₃COO⁻

Structure element	$\nu_s(\text{COO})$	$\delta(\text{H/DCO})$	$\nu_{as}(\text{COO})$	$\delta_s(\text{CH}_3)$	$\Delta\nu_{as-s}$
HCOO ⁻ (adsorbed) ^a	1349	1388	1540		191 ^b
HCOOH (adsorbed) ^c	1355	1377	1533		198
η^2 -(HCOO)Ti	1398–1412	1308–1312	1599–1633		200–221
η^1 -(HCOO)Ti	1228–1360	1386–1409	1657–1758		307–530
μ -(HCOO)Ti ₂ O ₂	1368–1396	1363–1399	1528–1674		204–303
μ -(HCOO)Ti ₅ O ₂ F ₂₀ ⁵⁻	1370	1385	1593		223
DCOO ⁻ (adsorbed) ^a	1322	1030	1534		212 ^b
η^2 -(DCOO)Ti	1362–1376	974–977	1577–1613		214–237
η^1 -(DCOO)Ti	1224–1341	1015–1033	1645–1732		312–508
μ -(DCOO)Ti ₂ O ₂	1335–1357	1016–1036	1511–1664		224–313
μ -(DCOO)Ti ₅ O ₂ F ₂₀ ⁵⁻	1342	1028	1580		238
CH ₃ COO ⁻ (adsorbed) ^a	1426		1513	1352	87 ^b
η^2 -(CH ₃ COO)Ti	1499–1504		1563–1577	1354–1359	58–79
η^1 -(CH ₃ COO)Ti	1405–1413		1660–1673	1326–1331	247–267
μ -(CH ₃ COO)Ti ₂ O ₂	1430–1483		1553–1618	1329–1366	69–188
μ -(CH ₃ COO)Ti ₅ O ₂ F ₂₀ ⁵⁻	1462		1569	1329	108

^a Adsorbed from aqueous solution, present ATR-FTIR data. ^b Experimental $\Delta\nu_{as-s}$ of the adsorbed component, obtained from the deconvoluted spectra. ^c Adsorbed from the gas phase, present ATR-FTIR data.

**Figure 16.** Perspective view of the μ -(HCOO)Ti₅O₂F₂₀⁵⁻ cluster (with C_{2v} symmetry).

by 47 and 48 cm⁻¹. By subtraction of this (most likely systematic) error, the calculated frequency would match the experimental value, but the error of *adsorbed* HCOO⁻ might be different from that of free HCOOH. In this cluster, the Ti–Ti distance is closest to the experimental value, the ordering of the $\nu_s(\text{COO})$ – $\delta(\text{HCO})$ – $\nu_{as}(\text{COO})$ modes is correct, and the deviation of calculated from experimental frequencies is smallest.

An alternative way of diminishing the strong trans effect exerted by the two fluoride ions trans to formate in the μ -(HCOO)Ti₂O₂F₆³⁻ cluster is to replace them by a second formate. The thus obtained μ -(HCOO)₂Ti₂O₂F₄²⁻ cluster has D_{2h} symmetry and a lower charge. Since two formate ions are present in the cluster, each of its mode is doubled, yielding a symmetric and an asymmetric species. This splitting varies from 1 to 24 cm⁻¹ for the modes listed in Table 2. With respect to μ -(HCOO)Ti₂O₂F₆³⁻ $\nu_s(\text{COO})$ increased by ~20 cm⁻¹, $\delta(\text{HCO})$ decreased by ~30 cm⁻¹, and $\nu_{as}(\text{COO})$ decreased by more than 50 cm⁻¹. The corresponding neutral cluster, μ -(HCOO)₂Ti₂F₆, in which the two bridging oxygens are replaced by fluoride, has lower $\nu_s(\text{COO})$ and $\nu_{as}(\text{COO})$ frequencies, but $\delta(\text{HCO})$ remains unchanged. Interestingly, in this uncharged cluster, $\nu(\text{CH})$ is in the expected range. However, at variance with experiment, $\delta(\text{HCO})$ is calculated at lower energy than $\nu_s(\text{COO})$ in these bis-formato clusters. Lowering of the charge yields shorter Ti–OOCH bonds, and the replacement of bridging oxygens by OH⁻ or F⁻ leads to a longer Ti–Ti distance.

It is interesting to note that in the mono-HCOO⁻ clusters, the Ti–OOCH distance varies from 2.042 to 2.283 Å (Table

2). The $\nu_{as}(\text{COO})$ and $\nu(\text{CH})$ frequencies depend linearly on d(Ti–OOCH), whereby $\nu_{as}(\text{COO})$ increases and $\nu(\text{CH})$ decreases with increasing d(Ti–OOCH).

The effect of H-bonding was investigated on the basis of dihydrates of the μ -(HCOO)Ti₃O₂F₁₀³⁻ and μ -(HCOO)Ti₃-(OH)₂F₁₀⁻ clusters, μ -(HCOO)Ti₃O₂F₁₀ · (H₂O)₂³⁻ (Figure 14b) and μ -(HCOO)Ti₃(OH)₂F₁₀ · (H₂O)₂⁻, both with C₂ symmetry. The $\delta(\text{OCO})$, $\pi(\text{H–COO})$, $\nu_s(\text{COO})$, and $\delta(\text{HCO})$ frequencies remain virtually unchanged, whereas $\nu_{as}(\text{COO})$ decreases by 9–10 cm⁻¹, and $\nu(\text{CH})$ increases by 9 or 38 cm⁻¹ (Table 2).

Other rutile clusters had strongly distorted structures that were very different from that of the rutile (110) surface (Figure 2), or the formate anion dissociated spontaneously.

(f) Adsorbed Acetate. For this carboxylic acid, a selection of the above-described HCOO⁻ structures was investigated, whereby the symmetry is lower, C_s except for the Ti₅ cluster for which it is C₁. The $\delta(\text{OCO})$ mode of acetate is calculated at lower frequencies than for HCOO⁻, and $\nu(\text{CC})$ – not observed experimentally – is in the range of 900–950 cm⁻¹ (Table 3).

Compared with HCOO⁻, the $\nu_s(\text{COO})$ and $\nu_{as}(\text{COO})$ modes are at higher and lower frequencies, respectively, which results in a lower $\Delta\nu_{as-s}$ for acetate compared with formate. The Ti–OOCCH₃ bonds are slightly shorter than the Ti–OOCH ones (Tables S2, S3, 2, and 3) due to the higher basicity of CH₃COO⁻. The η^2 and η^1 binding modes are unlikely for the same reasons as for HCOO⁻.

Summary of Diagnostic Calculated Frequencies. The $\nu(\text{CH})$, $\pi(\text{H–COO})$ and $\delta(\text{OCO})$ modes of HCOO⁻ were not observed in the ATR-FTIR measurements and will not be discussed further. In Table 4 are summarized the $\nu_s(\text{COO})$, $\delta(\text{H/DCO})$ and $\nu_{as}(\text{COO})$ modes calculated for the η^2 -(HCOO)-Ti, η^1 -(HCOO)Ti and μ -(HCOO)Ti₂ structure elements (Figure 1). Only the frequencies of structures that do not give rise to imaginary modes involving the HCOO⁻ anion are considered. It is remarkable that for the three η^2 -(HCOO)Ti structures fulfilling this criterion, the above 3 modes (Table 4) depend only slightly on the coordination number of Ti.

The IR intensities were also computed. In all clusters, the $\nu_{as}(\text{COO})$ band is the strongest, the intensity of $\nu_s(\text{COO})$ is about 1/3 to 1/2 of $\nu_{as}(\text{COO})$, $\delta(\text{HCO})$ is weaker than $\nu_s(\text{COO})$, and $\pi(\text{H–COO})$ weaker than $\delta(\text{HCO})$. In all of the binding modes, η^1 , η^2 , and μ , the IR intensities of the diagnostic frequencies are quite similar and, therefore, these data cannot be used for the determination of the surface binding mode of HCOO⁻.

For the acetate ion, the $\delta(\text{OCO})$, $\nu(\text{CC})$, and $\delta_{\text{as}}(\text{CH}_3)$ modes (Table 4) are not observed experimentally, and $\delta_{\text{s}}(\text{CH}_3)$ is not sensitive to the binding mode. Only the $\nu_{\text{s}}(\text{COO})$ and $\nu_{\text{as}}(\text{COO})$ modes are available for structure determination.

Discussion

Structure Assignment on the Basis of the $\nu_{\text{as}}(\text{COO}) - \nu_{\text{s}}(\text{COO})$ Difference, $\Delta\nu_{\text{as-s}}$. Most of the interpretation of interfacial infrared spectra measured in aqueous systems has been based on a comparison with vibrational spectra of transition metal complexes with known structure. Deacon, Huber, and Phillips,⁴³ and Deacon and Phillips,⁴⁴ have analyzed the positions of the asymmetric and symmetric carboxylate stretching vibrations, $\nu_{\text{as}}(\text{COO})$ and $\nu_{\text{s}}(\text{COO})$, and the separation between these vibrations, $\Delta\nu_{\text{as-s}}$, in a large number of acetate complexes. By comparing $\Delta\nu_{\text{as-s}}$ of free aqueous acetate, $\Delta\nu_{\text{as-s}}$ (ionic), to the $\Delta\nu_{\text{as-s}}$ values measured in the transition metal complexes, they have found the following correlation:^{43,44}

$\Delta\nu_{\text{as-s}} > \Delta\nu_{\text{as-s}}$ (ionic): \Rightarrow
monodentate coordination (η^1 coordination)

$\Delta\nu_{\text{as-s}} < \Delta\nu_{\text{as-s}}$ (ionic): \Rightarrow
chelating or bridging (η^2 or μ coordination)

$\Delta\nu_{\text{as-s}} \ll \Delta\nu_{\text{as-s}}$ (ionic): \Rightarrow chelating, unless short metal–
metal bonds are present (η^2 coordination)

The database examined strongly supports the first correlation as well as its converse. The first correlation is true in both directions – i.e., complexes showing $\Delta\nu_{\text{as-s}} > \Delta\nu_{\text{as-s}}$ (ionic) contain monodentate coordination, and complexes with monodentate coordination always show $\Delta\nu_{\text{as-s}} > \Delta\nu_{\text{as-s}}$ (ionic). The inverse of the second correlation, however, does not necessarily hold. Complexes with $\Delta\nu_{\text{as-s}} < \Delta\nu_{\text{as-s}}$ (ionic) generally have chelating and/or bridging coordination, but not every complex with chelating and/or bridging coordination shows $\Delta\nu_{\text{as-s}} < \Delta\nu_{\text{as-s}}$ (ionic). Nara et al., reported ab initio quantum mechanical calculations of the coordination of acetate to Na^+ , Mg^{2+} , and Ca^{2+} .⁵⁷ They also found $\Delta\nu_{\text{as-s}}$ (monodentate) $> \Delta\nu_{\text{as-s}}$ (ionic) $> \Delta\nu_{\text{as-s}}$ (chelating), while $\Delta\nu_{\text{as-s}}$ (bridging) was found to be larger or comparable to $\Delta\nu_{\text{as-s}}$ (ionic), depending on the metal. It should be noted that Nara et al.'s computations⁵⁷ involved metal ions with incomplete coordination spheres, while they are complete in all of the presently computed Ti^{IV} clusters.

The above-presented rules and correlations^{43,44} were based on transition metal carboxylato complexes with η^1 , η^2 and μ structures, *that exhibited different coordination numbers, charges and electron configurations of the metal*. The bond of a carboxylate anion to a transition metal ion involves both σ and π bonds, whose strengths depend on the number of d electrons in the corresponding d_{σ}^* and d_{π} molecular orbitals (MOs) of the metal center (d_{σ}^* : e_g^* , d_{π} : t_{2g} levels in octahedral symmetry). For example, Cr^{III} and Co^{III} have empty d_{σ}^* levels which give rise to strong metal–ligand bonds. The d_{π} levels, one of which is involved in the M–OOCR bond, are occupied by one or two electrons in Cr^{III} or Co^{III} complexes, respectively. As another example, carboxylato complexes of Ni^{II} and Cu^{II} exhibit partially occupied d_{σ}^* levels in addition to their filled d_{π} levels. It is obvious that the binding of carboxylate to Ti^{IV} , in which both, the d_{π} and d_{σ}^* MOs, are empty, is likely to be different from that of transition metal complexes with a partially filled d shell. The binding is expected to be again different for alkali and alkaline-earth metal ions because their d MOs, if they

are relevant at all, participate only weakly in the M–OOCR bonding. The charge of the metal center is also expected to affect the M–OOCR bond. As an important result, the computations (Tables S3 and 2) show that *especially $\nu_{\text{as}}(\text{COO})$ depends strongly on the environment of the metal*. The coupling of vibrations via off-diagonal elements in the force constant matrix also affects $\nu_{\text{as}}(\text{COO})$ and $\nu_{\text{s}}(\text{COO})$. The sign and magnitude of these matrix elements do not only depend on the geometry of the chromophore, but also on the electron density change that accompanies a given vibration. Since such factors are difficult to predict with empirical rules, the assignment of the binding mode on the basis of vibrational frequencies and empirical rules has to be made with care.

In aqueous solution, the C=O group of (hypothetical) η^1 -formate is likely to be hydrogen-bonded. Such interactions are known⁴⁴ to lower $\nu_{\text{as}}(\text{COO})$ and thus also $\Delta\nu_{\text{as-s}}$. The empirical rules^{43,44} were based on acetate; for other carboxylates such as formate, it was recommended⁴⁴ that they are applied in a more conservative manner.

For the adsorption of the formate and acetate ions to the (110) surface of TiO_2 , $\Delta\nu_{\text{as-s}}$ is smaller by 39 and 50 cm^{-1} , respectively, than $\Delta\nu_{\text{as-s}}$ (ionic). This suggests that for these two carboxylates, the η^1 binding mode is unlikely.

Structural Information From the Experimental Data. When nominally dry rutile surfaces are exposed to formic acid vapors, evidence for both molecular adsorption of formic acid as well as ionic adsorption of formate is seen (Figure 9). In contrast, no peaks above 1700 cm^{-1} indicative of C=O vibrations are observed for formate adsorbed to TiO_2 under aqueous conditions (Figure 8). This suggests that under aqueous conditions, adsorption of formic acid is minimal, while adsorption of the ionic formate dominates.

Adsorption results in clearly measurable spectral shifts, caused by specific chemical interactions with the surface. Surface associated components whose spectra do not differ appreciably from the aqueous components are likely nonspecifically (outer-sphere) adsorbed by electrostatic attraction and/or by weak hydrogen bonding. The specific differences between aqueous and adsorbed forms of formate and acetate observed in our spectra are a clear indication for specific interactions with direct bonding between the carboxylato group and Ti^{IV} surface sites.

Unlike single crystals, TiO_2 particles have less well defined surfaces, and multiple crystal faces might be exposed. In the presence of air or water, the surface is hydrated or hydroxylated. Infrared spectroscopic experiments on sufficiently dry TiO_2 samples (adsorbed water layers removed) show multiple absorbance peaks due to OH groups bound to titanium ions of different coordination number or local geometry.^{1,19} It is expected, therefore, that TiO_2 particles have a variety of chemically distinct sites at which organic molecules can adsorb. This is generally true for metal oxide surfaces and recent surface complexation models incorporated this complexity.^{58–60} In the rutile samples used in this study, the (110) faces constitute >95% of the exposed surfaces (Table 1), and there is predominantly one type of sites that is accessible for coordination with formate and acetate (Figure 2). In the measured spectra, there is no indication within signal-to-noise that more than one adsorbed structure with distinguishable vibrational features is formed.

The small differences in $\nu_{\text{as}}(\text{COO})$ and $\nu_{\text{s}}(\text{COO})$ arising from the adsorption of formate or formic acid from aqueous solution (Figure 8) or the gas phase (Figure 9), respectively, are most likely due to H-bonding and the protonation of oxygen coordinated to two Ti^{IV} centers (Figure 2).

The experimental data indicate that the formate and the acetate ions are adsorbed onto the Ti^{IV} sites in the same manner. A nonspecific simply electrostatic interaction can be ruled out on the basis of the frequency shifts of $\nu_{\text{as}}(\text{COO})$ upon adsorption (Figures 5 and 11). For formate, $\Delta\nu_{\text{as-s}}$ decreases from 230 to 191 cm⁻¹ upon adsorption to rutile (110); the change is 39 cm⁻¹. For acetate, $\Delta\nu_{\text{as-s}}$ diminishes by 50 cm⁻¹, from 137 cm⁻¹ to 87 cm⁻¹. According to the empirical rules derived by Deacon et al., this shift indicates a chelating (η^2) and/or bridging (μ) coordination. A η^1 coordination is unlikely because it would give rise to a substantial increase of $\Delta\nu_{\text{as-s}}$ with respect to $\Delta\nu_{\text{as-s}}(\text{ionic})$. The experimental data alone cannot be used to distinguish the η^2 from the μ structure. The rather large decrease of $\Delta\nu_{\text{as-s}}$ for both formate and acetate might suggest erroneously a chelating (η^2) coordination, but this binding mode is very unlikely because it would lead to hepta coordinated Ti^{IV} that is unstable with respect to η^1 coordination (see Results). In the present cases, Deacon et al.'s rules should not be used for the distinction of the η^2 and μ structures which are quite similar as the local symmetry of the carboxylate group is concerned.

Structure Derived From the Computations. The η^2 coordination (Figure 1a) of the formate and acetate ions on the (110) TiO₂ surface (Figure 2) can be ruled out because of the reasons discussed above. The calculations showed that hepta coordinated η^2 -formate and η^2 -acetate would be transition states (Figure 13). Hexa coordinated η^2 -formate is predicted to be stable, and this binding mode could exist on edges or corners. It would give rise to a $\delta(\text{HCO})$ frequency of about 1310 cm⁻¹ (Table S2), which is much lower than the experimental $\delta(\text{HCO})$ (Figure 5). According to density functional computations,⁶¹ hepta coordinated η^2 -formate is also unstable on the anatase (101) surface. Thus, the η^1 or the μ adsorption modes remain to be analyzed for the formate and acetate adsorption onto (110) rutile TiO₂.

Both, the $\nu_{\text{s}}(\text{COO})$ as well as the $\nu_{\text{as}}(\text{COO})$ stretching modes, depend strongly on the ligand trans to η^1 -bonded formate (Table S3). The weaker the Lewis basicity of the trans ligand, the larger the $\nu_{\text{as}}(\text{COO}) - \nu_{\text{s}}(\text{COO})$ splitting $\Delta\nu_{\text{as-s}}$: the replacement of F⁻ (or OH⁻) by H₂O causes an increase in $\nu_{\text{as}}(\text{COO})$ by ~70 cm⁻¹ and a decrease in $\nu_{\text{s}}(\text{COO})$ by ~95 cm⁻¹. Thus, $\Delta\nu_{\text{as-s}}$ increases by 167 cm⁻¹ from 363 to 530 cm⁻¹. The cis ligands exert a smaller influence on $\nu_{\text{as}}(\text{COO})$, $\nu_{\text{s}}(\text{COO})$, and $\Delta\nu_{\text{as-s}}$ showing that the Lewis basicity of these ligands affect $\nu_{\text{as}}(\text{COO})$ and $\nu_{\text{s}}(\text{COO})$ weakly. H-bonding with the solvent, modeled by two isomers of the monohydrates $\eta^1\text{-(HCOO)TiF}_5 \cdot \text{H}_2\text{O}^{2-}$ (Figs. S2b, c) has a small influence on the six modes of HCOO⁻ (Table S3). It is interesting to note that the $\delta(\text{HCO})$ mode is quite insensitive to both, the trans and the cis ligands, but it is considerably lower for the stable η^2 binding mode ($\eta^2\text{-(HCOO)-TiF}_4^-$ and $\eta^2\text{-(HCOO)TiF}_4 \cdot (\text{H}_2\text{O})_2^-$ clusters, Table S2). For η^1 formate, the computed and the experimental $\delta(\text{HCO})$ mode agrees, and so does also $\nu_{\text{s}}(\text{COO})$ (Table 3). The η^1 coordination is ruled out by the $\nu_{\text{as}}(\text{COO})$ mode whose lowest calculated values of 1663–1685 cm⁻¹, obtained with strong (in terms of Lewis basicity) trans ligands (F⁻, OH⁻), is higher than the experimental value by >120 cm⁻¹ or >70 cm⁻¹, if the systematic overestimation of $\nu_{\text{as}}(\text{COO}) \approx 50$ cm⁻¹ in HCOOH (Table S1) is taken into account. For a weaker trans ligand, this deviation is even larger. The η^1 coordination can be excluded because no $\eta^1\text{-(HCOO)Ti}^{\text{IV}}$ cluster was found that has a sufficiently low $\nu_{\text{as}}(\text{COO})$ mode, and because the computed value of $\Delta\nu_{\text{as-s}}$ is much larger than the experimental one as well as $\Delta\nu_{\text{as-s}}(\text{ionic})$. Upon deuteration of the formate ion, the measured ($\Delta\nu_{\text{as-s}})_{\text{ads}}$ value increases by 21 cm⁻¹.

According to the calculations on the $\eta^1\text{-H/DCOO}^-$ structures, $\Delta\nu_{\text{as-s}}$ increases marginally (by ≤ 8 cm⁻¹) or decreases (Table S3), whereas for the η^2 - and the $\mu\text{-H/DCOO}^-$ structures, $\Delta\nu_{\text{as-s}}$ increases by 10–16 cm⁻¹ (Table S2) and 10–20 cm⁻¹ (Table 2), respectively.

For η^1 bound acetate, the situation is similar: the $\nu_{\text{s}}(\text{COO})$ value is close to the experimental one, whereas $\nu_{\text{as}}(\text{COO})$ is computed at much higher frequencies, yielding a too large $\Delta\nu_{\text{as-s}}$ (Table 3).

The exclusion of the η^1 and the η^2 binding modes leaves the μ coordination as the only and last possibility. In the following, it will be shown that indeed the computations argue in favor of μ binding. In all of the $\mu\text{-(HCOO)Ti}_{2,3,5}$ clusters, $\delta(\text{HCO})$ is close to the experimental value (Tables 2 and 3), and so is the calculated $\nu_{\text{s}}(\text{COO})$ mode. In some clusters, at variance with experiment, $\delta(\text{HCO})$ is lower than $\nu_{\text{s}}(\text{COO})$ because $\delta(\text{HCO})$ is too low (by ≤ 25 cm⁻¹) and $\nu_{\text{s}}(\text{COO})$ is too high (by ≤ 47 cm⁻¹). These clusters, however, give rise to more accurate $\nu_{\text{as}}(\text{COO})$ modes than most of the clusters with the correct $\delta(\text{HCO}) - \nu_{\text{s}}(\text{COO})$ order. The $\mu\text{-(HCOO)Ti}_5\text{O}_2\text{F}_{20}^{5-}$ cluster (Figure 16) yields computed vibrational frequencies in the right order that are close to the experimental values. It should be recalled that the computed $\nu_{\text{as}}(\text{COO})$ modes of *cis*- and *trans*-HCOOH are too high by 47–48 cm⁻¹ (Table S1). The inclusion of H-bonding lowers $\nu_{\text{as}}(\text{COO})$ by ~10–20 cm⁻¹ (Table 2). If these two factors (the systematic error in $\nu_{\text{as}}(\text{COO})$ and the neglect of H-bonding) are taken into account, the frequencies of the $\mu\text{-(HCOO)Ti}_5\text{O}_2\text{F}_{20}^{5-}$ cluster agree with experiment. In this case, the $\nu_{\text{as}}(\text{COO})$ deviation is much smaller than that for the η^1 coordination. For the $\mu\text{-(HCOO)}$ clusters, the $\delta(\text{HCO})$ and $\nu_{\text{s}}(\text{COO})$ frequencies are quite insensitive to the trans as well as the cis ligands. Only $\nu_{\text{as}}(\text{COO})$ depends strongly on the environment of the metal and varies by about 150 cm⁻¹ (Table 2).

The cluster calculations clearly favor the μ coordination on the basis of the agreement of the $\delta(\text{HCO})$ and $\nu_{\text{s}}(\text{COO})$ bands with experiment, as well as $\nu_{\text{as}}(\text{COO})$, if the systematic error in the computation of this mode is taken into account. It should be remembered, that the present clusters are only approximations to the (110) surface, that hydrogen bonding has been included using a rather simple model, and that the computational method is not the most accurate one, although it is the best for such large systems. MP2 computations are prohibitive for the larger clusters and possibly not even adequate because of static electron correlation: a good description of the ionic Ti–O and Ti–F bonds would require at least a multireference MP2 technique.

Also, for acetate in the μ binding mode, the computed $\nu_{\text{as}}(\text{COO})$ frequency is too high compared with experiment, whereas $\delta_{\text{s}}(\text{CH}_3)$ and $\nu_{\text{s}}(\text{COO})$ are close to their respective experimental values. The measured as well as the computed data indicate that formate and acetate bind to the rutile TiO₂ (110) surface in the same way.

Comparison with Other Work. The present experimental ATR-FTIR data, together with the computed frequencies, suggest that formate and acetate adsorb via the bridging bidentate (μ) structure (Figure 1c). The available literature, experimental work on the adsorption of the acid from the gas phase as well as theoretical studies, suggests also a μ coordination for formate and acetate adsorbed onto the TiO₂ rutile (110) surface.

Photoelectron diffraction in both scanned-angle and scanned-energy modes, combined with HF calculations³¹ supply evidence for the μ structure, in which the two oxygens of formate bind to Ti in [001] rows. A scanning tunneling microscopic study

indicates that formate is adsorbed via the bridging bidentate (μ) structure.³⁴ The same authors corroborated this result in an atomic force microscopy investigation.³³ A theoretical study⁴⁰ suggests that formic acid is most favorably adsorbed onto the rutile (110) surface in the bridging bidentate (μ) mode, whereby the proton is transferred to basic O sites on the surface. First-principles calculations⁴¹ based on density functional theory on 5 possible structures show that the deprotonated bridging bidentate (μ) mode is most stable, whereby, as in the previously mentioned study, the proton is transferred to the basic O sites of the (110) surface. Later, this prediction has been established by X-ray photoelectron spectroscopy and Fourier transform reflection–absorption IR spectroscopy.³²

The structure of acetic acid adsorbed onto the rutile (110) surface has been determined^{37,40} using electron stimulated desorption ion angular distribution and low energy electron diffraction. Acetic acid adsorbs dissociatively forming the μ structure as formic acid.

Conclusions

The adsorption of formate and acetate from aqueous solutions to the rutile (110) TiO_2 surface has been shown to involve a specific, reversible interaction of the carboxylate groups with the TiO_2 surface. According to the frequency computations, these two carboxylates form the bridging bidentate (μ) structures (Figure 1c) under aqueous conditions (as in the adsorption of the acid from the gas phase). The monodentate (η^1) structure (Figure 1b) can be ruled out because it would have a much higher $\nu_{\text{as}}(\text{COO})$ frequency, whereas the chelating bidentate (η^2) structure (Figure 1a) on pentacoordinated Ti^{IV} in the (110) surface is unstable with respect to the rearrangement to the η^1 or μ structure and for formate, it would, furthermore, give rise to a much lower $\delta(\text{HCO})$ frequency.

For the present systems, the same adsorbed structures of formate and acetate are found for the aqueous and the “dry” gas-phase systems.

Acknowledgment. The HRTEM work was performed at the Laboratory of Solid State Physics (ETH Hönggerberg). High specific surface area rutile was a gift from Sachtleben Chemie GmbH. The Swiss National Science Foundation is acknowledged for financial support (NRP 47). J. M. Kesselman-Truttmann gratefully acknowledges the support of the U. S. National Science Foundation for an International Research Fellow Award.

Supporting Information Available: The structures of the η^2 –, η^1 –, and other $\mu\text{-HCOO}^- \text{Ti}^{\text{IV}}$ clusters are shown in Figures S1–S4. The experimental and calculated vibrational frequencies of free *cis*- and *trans*- HCOOH (in the gas phase) are given in Table S1. The computed frequencies of the η^2 – and η^1 – $\text{HCOO}^- \text{Ti}^{\text{IV}}$ clusters are reported in Tables S2 and S3. This material is available free of charge via the Internet at <http://pubs.acs.org>.

References and Notes

- (1) Hadjiivanov, K. I.; Klissurski, D. G. *Chem. Soc. Rev.* **1996**, 25, 61.
- (2) Hoffmann, M. R.; Martin, S. T.; Choi, W.; Bahnemann, D. W. *Chem. Rev.* **1995**, 95, 69.
- (3) Linsebigler, A. L.; Lu, G.; Jr., J. T. Y. *Chem. Rev.* **1995**, 95, 735.
- (4) Matthews, R. W. *Wat. Res.* **1986**, 20, 569.
- (5) Ollis, D. F.; Pelizzetti, E.; Serpone, N. 344. Heterogeneous Photocatalysis in the Environment: Application to Water Purification. In *Photocatalysis: Fundamentals and Applications*; Serpone, N., Pelizzetti, E., Eds.; John Wiley & Sons: New York, 1989; pp 603–637.
- (6) Cunningham, J.; Al-Sayyed, G.; Sedláč, P.; Caffrey, J. *Catal. Today* **1999**, 53, 145.
- (7) Cunningham, J.; Sedláč, P. *J. Photochem. Photobiol. A: Chem.* **1994**, 77, 255.
- (8) Grätzel, M. *MRS Bulletin* **1993**, 61.
- (9) Grätzel, M.; Kalyanasundaram, K. *Current Science* **1994**, 66, 706.
- (10) O'Regan, B.; Grätzel, M. *Nature* **1991**, 353, 737.
- (11) Grätzel, M. *Nature* **2001**, 414, 338.
- (12) Murakoshi, K.; Kano, G.; Wada, Y.; Yanagida, S.; Miyazaki, H.; Matsumoto, M.; Murasawa, S. *J. Electroanal. Chem.* **1995**, 396, 27.
- (13) Tachibana, Y.; Moser, J. E.; Grätzel, M.; Klug, D. R.; Durrant, J. R. *J. Phys. Chem.* **1996**, 100, 20056.
- (14) Argazzi, R.; Bignozzi, C. A.; Heimer, T. A.; Castellano, F. N.; Meyer, G. J. *Inorg. Chem.* **1994**, 33, 5741.
- (15) Davydov, A. A. 345. *Infrared Spectroscopy of Adsorbed Species on the Surface of Transition Metal Oxides*; John Wiley & Sons: Chichester, 1990.
- (16) Primet, M.; Pichat, P.; Mathieu, M.-V. *J. Phys. Chem.* **1971**, 75, 1221.
- (17) Primet, M.; Pichat, P.; Mathieu, M.-V. *J. Phys. Chem.* **1971**, 75, 1216.
- (18) Chambers, S. A.; Thevuthasan, S.; Kim, Y. J.; Herman, G. S.; Wang, Z.; Tober, E.; Ynzunza, R.; Morais, J.; Peden, C. H. F.; Ferris, K.; Fadley, C. S. *Chem. Phys. Lett.* **1997**, 267, 51.
- (19) Wang, L.-Q.; Ferris, K. F.; Shultz, A. N.; Baer, D. R.; Engelhard, M. H. *Surf. Sci.* **1997**, 380, 352.
- (20) Cocks, I. D.; Guo, Q.; Patel, R.; Williams, E. M.; Roman, E.; Segovia, J. L. d. *Surf. Sci.* **1997**, 377–379, 135.
- (21) Hind, A. R.; Bhargava, S. K.; McKinnon, A. *Adv. in Coll. and Interface Sci.* **2001**, 93, 91.
- (22) Hug, S. J.; Sulzberger, B. *Langmuir* **1994**, 10, 3587.
- (23) Connor, P. A.; Dobson, K. D.; McQuillan, J. *Langmuir* **1995**, 11, 4193.
- (24) Tunesi, S.; Anderson, M. A. *Langmuir* **1992**, 8, 487.
- (25) Martin, S. T.; Kesselman, J. M.; Park, D. S.; Lewis, N. S.; Hoffmann, M. R. *Environ. Sci. Technol.* **1996**, 30, 2535.
- (26) Weisz, A. D.; Regazzoni, A. E.; Blesa, M. A. *Solid State Ionics* **2001**, 143, 125.
- (27) Kesselman-Truttmann, J. M.; Hug, S. J. *Environ. Sci. Technol.* **1999**, 33, 3171.
- (28) Nazeeruddin, M. K.; Kay, A.; Rodicio, I.; Humphry-Baker, R.; Müller, E.; Liska, P.; Vlachopoulos, N. *J. Am. Chem. Soc.* **1993**, 115, 6382.
- (29) Baur, W. H. *Acta Crystallogr.* **1961**, 14, 209.
- (30) Cromer, D. T.; Herrington, K. J. *Am. Chem. Soc.* **1955**, 77, 4708.
- (31) Chambers, S. A.; Thevuthasan, S.; Kim, Y. J.; Herman, G. S.; Wang, Z.; Tober, E.; Ynzunza, R.; Morais, J.; Peden, C. H. F.; Ferris, K.; Fadley, C. S. *Chem. Phys. Lett.* **1997**, 267, 51.
- (32) Hayden, B. E.; King, A.; Newton, M. A. *J. Phys. Chem. B* **1999**, 103, 203.
- (33) Fukui, K.; Onishi, H.; Iwasawa, Y. *Chem. Phys. Lett.* **1997**, 280, 296.
- (34) Onishi, H.; Fukui, K.; Iwasawa, Y. *Coll. and Surf. A* **1996**, 109, 335.
- (35) Chambers, S. A.; Henderson, M. A.; Kim, Y. J.; Thevuthasan, S. *Surf. Rev. Lett.* **1998**, 5, 381.
- (36) Gutiérrez-Sosa, A.; Martínez-Escobedo, P.; Raza, H.; Lindsay, R.; Wincott, P. L.; Thornton, G. *Surf. Sci.* **2001**, 471, 163.
- (37) Guo, Q.; Cocks, I.; Williams, E. M. *J. Chem. Phys.* **1997**, 106, 2924.
- (38) Fukui, K.; Iwasawa, Y. *Surf. Sci.* **2000**, 464, L719.
- (39) Guo, Q.; Williams, E. M. *Surf. Sci.* **1999**, 433–435, 322.
- (40) Ahdjoudj, J.; Minot, C. *Catal. Lett.* **1997**, 46, 83.
- (41) Bates, S. P.; Kresse, G.; Gillan, M. J. *Surf. Sci.* **1998**, 409, 336.
- (42) Käckell, P.; Terakura, K. *Surf. Sci.* **2000**, 461, 191.
- (43) Deacon, G. B.; Huber, F.; Phillips, R. J. *Inorg. Chim. Acta* **1985**, 104, 41.
- (44) Deacon, G. B.; Phillips, R. J. *Coord. Chem. Rev.* **1980**, 33, 227.
- (45) Schmidt, M. W.; Baldrige, K. K.; Boatz, J. A.; Elbert, S. T.; Gordon, M. S.; Jensen, J. H.; Koseki, S.; Matsunaga, N.; Nguyen, K. A.; Su, S. J.; Windus, T. L.; Dupuis, M.; Montgomery, J. A. *J. Comput. Chem.* **1993**, 14, 1347.
- (46) Stevens, W. J.; Krauss, M.; Basch, H.; Jasien, P. G. *Can. J. Chem.* **1992**, 70, 612.
- (47) Hehre, W. J.; Ditchfield, R.; Pople, J. A. *J. Chem. Phys.* **1972**, 56, 2257.
- (48) Ditchfield, R.; Hehre, W. J.; Pople, J. A. *J. Chem. Phys.* **1971**, 54, 724.
- (49) Schäfer, A.; Horn, H.; Ahlrichs, R. *J. Chem. Phys.* **1992**, 97, 2571.
- (50) Millikan, R. C.; Pitzer, K. S. *J. Chem. Phys.* **1957**, 27, 1305.
- (51) Hisatsune, J. C.; Heicklen, J. *Can. J. Spectrosc.* **1973**, 18, 77.
- (52) Pettersson, M.; Lundell, J.; Khriachtchev, L.; Räsänen, M. *J. Am. Chem. Soc.* **1997**, 119, 11715.

- (53) In many cases, the analytical Hessian calculations produced erroneous results, presumably because of the low-lying 3d MOs of Ti^{IV}. In these cases, the second derivatives had to be computed numerically.
- (54) Miller, W. H.; Handy, N. C.; Adams, J. E. *J. Chem. Phys.* **1980**, 72, 99.
- (55) Nakamoto, K. 819. *Infrared and Raman Spectra of Inorganic and Coordination Compounds*, Fourth ed.; John Wiley & Sons: New York.
- (56) Munuera, G. *J. Catalysis* **1970**, 18, 19.

- (57) Nara, M.; Torii, H.; Tasumi, M. *J. Phys. Chem.* **1996**, 100, 19812.
- (58) Hiemstra, T.; Riemsdijk, W. H. V.; Bolt, G. H. *J. Coll. Int. Sci.* **1989**, 133, 91.
- (59) Hiemstra, T.; Wit, J. C. M. D.; Riemsdijk, W. H. V. *J. Coll. Int. Sci.* **1989**, 133, 105.
- (60) Hiemstra, T.; Riemsdijk, W. H. V. *J. Coll. Int. Sci.* **1996**, 179, 488.
- (61) Vittadini, A.; Selloni, A.; Rotzinger, F. P.; Grätzel, M. *J. Phys. Chem. B* **2000**, 104, 1300.